KRONOS FUSION ENERGY

PAPER 2.45 · THE KRONOS 2026 SERIES

# *Pellet Fueling, Particle Balance, and Helium-Ash Exhaust for Sustained Burn in a Compact Spherical-Tokamak Breeder*

A compact breeder that holds its burn must fuel the core, hold the operating density, and clear the helium ash it makes—all at once and inside a single wall-load budget. We report...

Read it live — 3-D model · physics validator · film series

BY P I FORDOFFICIAL VERSION: KRONOSFUSIONENERGY.COM/PUBLICATIONS/PELLET-FUELING-PARTICLE-BALANCE-AND-HELIUM-ASH-EXHAUST AND G L KULCINSKI

2026 · EDITORIAL EDITION

THE OFFICIAL RECORD

# What this document is, and how to read its numbers

This is a combined editorial. It gathers, in one volume, the two design studies Kronos Fusion Energy released in 2026 — a compact spherical-tokamak tritium/helium-3 breeder and a deuterium–helium-3 tandem-mirror generator — together with the intellectual-property estate, the people, and, in the internal edition, the full commercial case. The scientific text is the same text that appears in the arXiv preprints and the journal submissions; the editorial adds the apparatus a reader needs to hold the whole program at once, and nothing in the physics is altered to fit it.

## THE HONESTY STANCE IS THE ASSET

Every headline quantity carries an **evidence class** — DERIVED RECOMPUTED MEASURED REQUIREMENT — and, where a number is a modelled extrapolation rather than a demonstrated value, it is labelled as such and its downside is shown next to it. Several quantities in the underlying corpus moved after first publication; where a value has been withdrawn or restated, the record says so plainly. This is deliberate: a diligence team will find the load-bearing assumptions, so the document surfaces them first.

## TWO EDITIONS

This volume is issued in two editions. The **public edition** (light) carries the physics and the design only — no dollar, price, or per-kilogram figure appears anywhere in it. The **internal edition** (dark) adds the economics, the funding architecture, and the defense-commercial analysis, and is marked *Confidential* accordingly; it is not for public distribution. Where the commercial case rests on a modelled assumption rather than a demonstrated one, it is labelled as such and its downside is shown alongside it, on the same terms as the physics.

| | |
|---|---|
| TITLE | The Kronos Fleet — Hyperion · Aegis · MetroVolt: A Combined Design & Commercialization Study |
| AUTHOR | Priyanca Ford, Founder & CEO, on behalf of Kronos Fusion Energy |
| EDITION | 2026 Combined Editorial · first issue |
| COMPANION WORKS | The five-paper arXiv drop — (1) Breeder, (2) Burner, (3) REBCO magnet & tape, (4) Direct Energy Conversion, (5) AI/ML/Quantum control — with matching numbered Zenodo deposits, plus the IOP journal and IAEA-FEC submissions. Patents were filed before the drop. |
| NAMING | Hyperion = the breeder; Aegis (defense) and MetroVolt (data-center) = one generator in two housings. Internal mode letters (D1, L) do not appear on public surfaces. |
| STATUS | Conceptual design & simulation study. Nothing herein is a construction commitment. |

HOW TO READ THIS VOLUME

# The fleet at a glance, and the way its numbers are marked

This volume opens with *Orientation*, presents the five research papers as a bound sequence, and closes with the *Apparatus*. *Foundations* sets out the three general results both machines rest on. *Paper One* is the Hyperion breeder; *Paper Two* the Aegis / MetroVolt generator; *Papers Three, Four and Five* are the enabling science — high-field REBCO magnets and tape, direct energy conversion, and the AI / ML / quantum control stack. A *Digital Twin & 3-D Model* part follows, then the *Environmental* profile. The *Economics* and levelized cost and the *Business Case* and diligence record appear in the internal edition only; the *Simulations* proof record and the Apparatus — patent portfolio, team, limitations, and sources — close both editions.

## THE FLEET AT A GLANCE

| | HYPERION | AEGIS | METROVOLT |
|---|---|---|---|
| **Role** | Strategic-isotope foundry | Defense installation power | Campus power |
| **Machine** | **Spherical tokamak** | **Tandem mirror** | **Tandem mirror** |
| **Fuel** | Deuterium–tritium | Deuterium–helium-3 | Deuterium–helium-3 |
| **Delivers** | Tritium · $^{3}$He · 14 MeV n | Resilient installation power | Firm campus power |
| **Physics bar** | **Fusion gain only** | Closure (gates named) | Closure + lunar $^{3}$He |
| **In the fleet** | Breeds the fuel | Proves the generator | Commercial destination |

## HOW THE NUMBERS ARE MARKED

Every headline quantity carries an evidence class — DERIVED from first principles, RECOMPUTED from raw data, MEASURED in hardware, or a REQUIREMENT yet to be met. Financial figures carry a case label and are confined to the internal (confidential) edition. Values that moved after first publication are shown as withdrawn or restated rather than quietly changed. A capability you can evaluate is one whose limits are on the page.

ABSTRACT

# Pellet Fueling, Particle Balance, and Helium-Ash Exhaust for Sustained Burn in a Compact Spherical-Tokamak Breeder

A compact breeder that holds its burn must fuel the core, hold the operating density, and clear the helium ash it makes—all at once and inside a single wall-load budget. We report the closed particle balance for the Hyperion breeder at its frozen design point ( $P_{\text{fus}} = 85.04\, MW$, $I_p = 9.66\, MA$, $Q = 3.076$, negative triangularity $\delta = -0.30$, $B_0 = 8\, T$, $\kappa = 2.0$, $R_0 = 1.20\, m$, aspect ratio $A = 2.5$), cast as a coupled species continuity problem and solved on the Kronos GPU-HPC campaign. At full power the core produces helium (alpha) ash and burns D–T ions at $S_\alpha = 3.02 \times 10^{19}\, \text{s}^{-1}$ and $6.03 \times 10^{19}\, \text{s}^{-1}$; orbit-following (ASCOT5, $10^5$ markers) places $99.99\%$ of the alphas on confined orbits—a prompt loss of $0.013$–$0.023\%$ and a first-wall alpha load of $0.08$–$0.22\, \text{kW}\, \text{m}^{-2}$—so essentially every alpha thermalizes into ash that the divertor must exhaust. We show the operating density is set not by the classical Greenwald gas limit but by the first-wall neutron budget: gas fueling reaches a density fraction $f_G \approx 0.45$, while holding the neutron wall load fixed caps the useful band at $f_G \approx 0.36$ (a $+38\%$ neutron penalty at the higher density). Within that ceiling, pellet injection buys core *peaking* rather than average density: because the fusion rate scales as $\langle n^2 \rangle$, a peaking factor $p = n_0/\langle n \rangle$ delivers a fusion-rate gain $p^2/(2p-1)$—$\times 1.33$ at $p = 2$, $\times 1.80$ at $p = 3$—at fixed volume-average density and hence fixed wall load. We close the helium balance as $n_{\text{He}} V / \tau^*_{\text{He}} = S_\alpha$, which caps the tolerable effective ash confinement time at $\tau^*_{\text{He}} \lesssim 8.7\, s$ for a $5\%$ ash fraction, and we tie the fueling rate to the operating-current-window controller that holds $I_p \in [8.78, 9.66]\, \text{MA}$ against the centrepost-life ceiling. The result is a consistent, source-to-exhaust particle balance in which fueling method, density ceiling, and ash removal are governed by the one wall-load constraint that also governs the rest of the machine.

Open-access deposit (code & data, CC BY 4.0): DOI 10.5281/zenodo.22645848 · Zenodo community *kronos_fusion_energy*. Explore it live: interactive 3-D model · physics validator.

**Keywords:** pellet fueling · Greenwald density limit · helium-ash exhaust · particle balance · alpha confinement · spherical-tokamak breeder

CONTENTS

# Table of Contents

NOMENCLATURE

# Symbols, units, and the names of things

| | |
|---|---|
| $Q$ | plasma (fusion) gain, $P_{fus}/P_{aux}$ |
| $Q_E$ | engineering gain, net electric out / recirculating in |
| $H_{98}$ | confinement enhancement over the IPB98(y,2) scaling |
| $Z_{eff}$ | effective ion charge |
| $c_{ee}$ | electron–electron bremsstrahlung leading coefficient, 2.120022 (exact) |
| $\tau_E$ | energy confinement time |
| $I_p$ | plasma current |
| $R_0, a$ | major radius, minor radius |
| $\kappa, \delta$ | elongation, triangularity |
| $\beta_N$ | normalized plasma beta (Troyon-normalized) |
| *TBR* | tritium breeding ratio |
| *DEC* | direct energy conversion |
| *CF* | plant capacity factor (availability) |
| *FOAK / NOAK / BOAK* | first / $n^{th}$ / best of a kind |
| *Hyperion* | the ST breeder (internal: Mode D2) |
| *Aegis* | the generator, defense/installation housing (internal: Mode M) |
| *MetroVolt* | the generator, data-center housing (Mode M) |

§ 1

# Introduction

## THE PARTICLE ECONOMY OF A COMPACT BREEDER

The Hyperion breeder holds $I_p = 9.66\,MA$ of plasma current at a major radius of only $R_0 = 1.20\,m$ behind a centrepost magnet at a peak field of 16.84 T, in a negative-triangularity ($\delta = -0.30$) regime, producing $P_{\text{fus}} = 85.04\,MW$ at $Q = 3.076$ [1]. A device this compact makes fusion power—and helium ash—in a small plasma volume ($V \approx 10.9\,m^3$; see §2), so the particle economy is tight. Three requirements must be met simultaneously and are physically coupled: (i) the fueling system must deliver deuterons and tritons to the core faster than they burn or diffuse out, (ii) the operating line density must sit at the value the power balance assumes without tripping a wall or stability limit, and (iii) the divertor and pumping train must remove the helium the reactions leave behind at the rate the core makes it, or the ash fraction climbs and dilutes the fuel. This paper reports that balance end to end, from the fueling source through the density ceiling to the ash exhaust, and grounds each step in the frozen design-point calculations of the Kronos Physics De-Risking Register [1], whose serial identifiers (e.g. BR-CX-09) are cited inline so that every number is auditable.

## PRIOR ART

Fueling, density control and helium exhaust are each mature subjects. Pellet injection as a core-fueling technique was placed on a quantitative footing by the neutral-gas-shielding (NGS) ablation theory of Parks and Turnbull [9] and reviewed comprehensively by Milora *et al.* [10] and later by P\'egouri\'e [11]; the enabling experimental result—that high-field-side (HFS) launch deposits mass far deeper than low-field-side (LFS) launch despite lower pellet speed, producing strongly peaked density profiles—was demonstrated on DIII-D [12] and exploited for high-density, all-metal-wall operation on ASDEX Upgrade [13]. The operating-density ceiling is classically the Greenwald empirical limit [7], but for a nuclear device the binding constraint is often not the disruptive gas limit but the neutron wall load. Helium-ash removal has been studied since the first burning-plasma projections: Reiter *et al.* framed the exhaust requirement through an effective helium confinement time and a divertor enrichment factor [14,15], and dedicated exhaust experiments on TEXTOR [16] and DIII-D [17] demonstrated helium removal at time constants of order $10$–$20$ energy-confinement times, consistent with the requirements later codified in the ITER Physics Basis [18]. Core particle transport that converts a given deposition profile into an achieved peaking factor is set by turbulent convection and the anomalous pinch [19].

## CONTRIBUTION

What is missing for a compact nuclear spherical tokamak (ST)—which combines a very high current density, a hard first-wall neutron budget, and a consumable centrepost—is a single, closed particle balance that (i) states the source-to-exhaust budget as coupled continuity equations grounded in the frozen operating point, (ii) shows quantitatively that the neutron wall load rather than the Greenwald fraction sets the density ceiling, (iii) quantifies exactly what pellet injection buys over gas at that ceiling, and (iv) fixes the helium-exhaust requirement and ties the fueling actuation to the machine's other constraints. This paper contributes that balance. We give the geometry and rate budget (§2); the governing continuity equations for the fuel and ash species, the helium steady-state with enrichment, the Greenwald-versus-wall-load argument, and the NGS pellet-ablation model (§3); the numerical formulation of the one-dimensional flux-surface-averaged transport solver, its finite-volume discretization and convergence (§4); the GPU-HPC campaign that produced the results (§5); the results with eight data figures and the peaking analysis (§6); a quantitative comparison to the published helium-exhaust and pellet-fueling literature (§7); one honest open item (§8); and the conclusion (§9).

§ 2

# Geometry and the steady-state rate budget

The plasma occupies an elongated D-shaped cross-section of minor radius $a = R_0/A = 0.48\,m$ and elongation $\kappa = 2.0$. Approximating the flux surfaces as nested ellipses, the plasma volume is

$$V = 2\pi^2\, R_0\, a^2\, \kappa = 2\pi^2(1.20)(0.48)^2(2.0) = 10.9\,\mathrm{m}^3.$$

Each D–T reaction yields one $3.5\,MeV$ alpha and one $14.1\,MeV$ neutron, carrying $E_{\mathrm{fus}} = 17.6\,MeV = 2.82e-12\,J$ of total energy. The reaction rate implied by the frozen fusion power is therefore

$$R_{\mathrm{rx}} = \frac{P_{\mathrm{fus}}}{E_{\mathrm{fus}}} = \frac{85.04e6\,\mathrm{W}}{2.82e-12\,\mathrm{J}} = 3.02\times10^{19}\,\mathrm{s}^{-1},$$

which is simultaneously the alpha (helium-ash) production rate $S_\alpha = R_{\mathrm{rx}}$ and, doubled, the D–T ion burn rate $\dot{N}_{\mathrm{burn}} = 2R_{\mathrm{rx}} = 6.03\times10^{19}\,\mathrm{s}^{-1}$ that fueling must replace against burn-up (BR-L1-A1) [1]. This rate is consistent with the underlying Bosch–Hale D–T reactivity [8] folded over the frozen density and temperature profiles. Orbit-following of the fusion alphas—evaluated first with the in-house guiding-centre follower (BR-L1-A14) and arbitrated with ASCOT5 at $10^5$ markers (BR-L2-A20) [20,1]—places $99.99\%$ of them on confined orbits, with a prompt loss of $0.013$–$0.023\%$ and a mean first-wall alpha load of $0.08$–$0.22\,\mathrm{kW\,m^{-2}}$ (peak $1.94\,kW/m^2$). Well-confined alphas are exactly what a burning plasma wants for self-heating—but it also means almost every alpha slows down in the core and becomes thermal helium ash that must be actively removed rather than lost promptly to the wall. Table 1 collects the steady-state budget; figure 1 plots the rates.

| QUANTITY | VALUE | SOURCE |
|---|---|---|
| **fusion power $P_{\mathrm{fus}}$** | 85.04 MW | frozen anchor (BR-L1-A1) |
| **plasma volume $V$** | $10.9\,\mathrm{m}^3$ | eq. (1) |
| **alpha (He-ash) production $S_\alpha$** | $3.02\times10^{19}\,\mathrm{s}^{-1}$ | eq. (2) |
| **D–T ion burn rate $\dot{N}_{\mathrm{burn}}$** | $6.03\times10^{19}\,\mathrm{s}^{-1}$ | $2R_{\mathrm{rx}}$ |
| **alpha confined fraction** | 99.99% | BR-L1-A14 / BR-L2-A20 |
| **prompt alpha loss** | 0.013–0.023% | BR-L1-A14 / A20 |
| **first-wall alpha load** | $0.08$–$0.22\,\mathrm{kW\,m^{-2}}$ | BR-L2-A20 |
| **Greenwald density $n_{\mathrm{GW}}$** | $1.33\times10^{21}\,\mathrm{m}^{-3}$ | eq. (12) |
| **gas-fueling density fraction** | $f_G \approx 0.45$ | BR-CX-09 |
| **first-wall-limited band** | $f_G \approx 0.36$ | BR-CX-09 |

Steady-state particle budget at the frozen breeder design point. Rates follow from $P_ fus=§I85.04

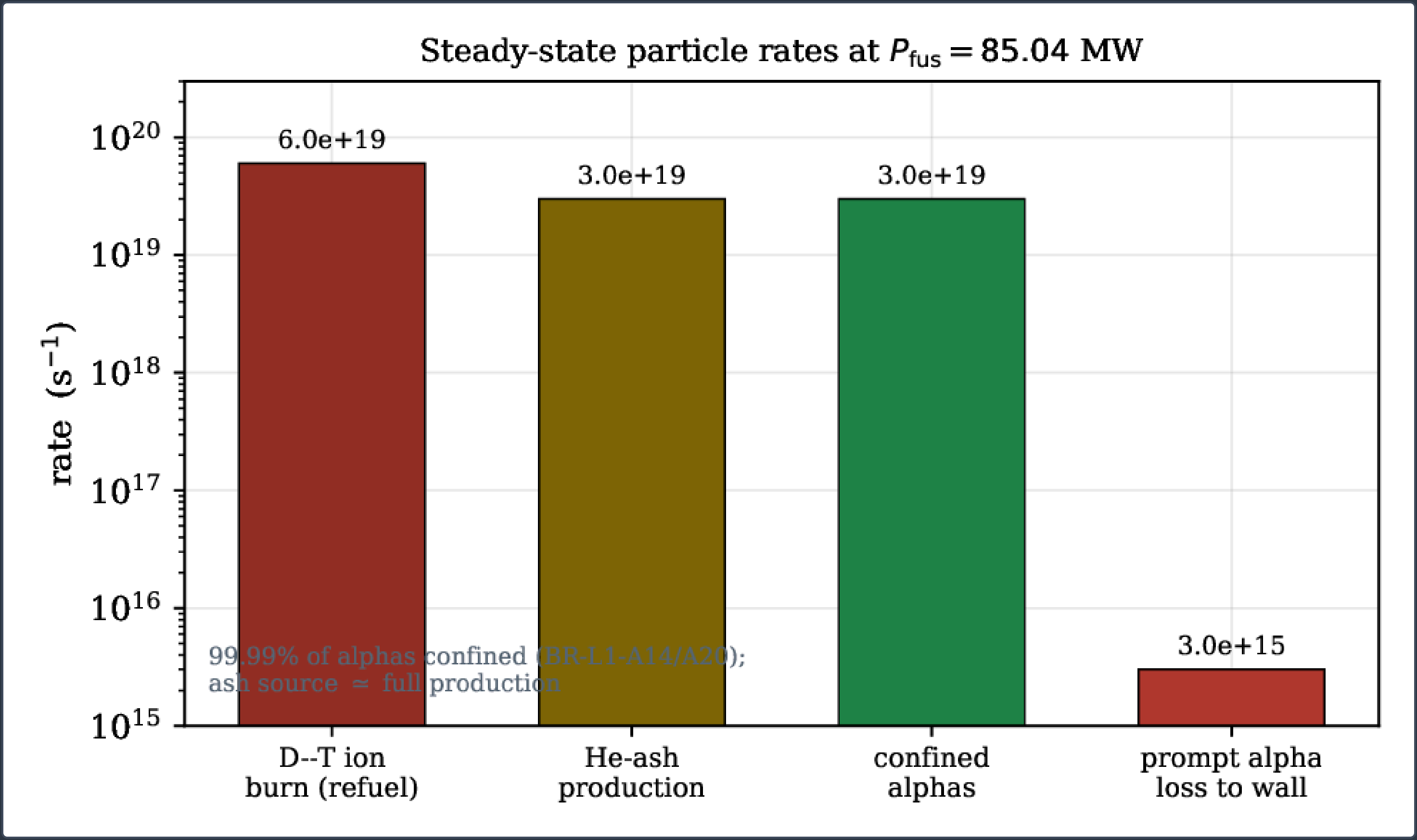


Steady-state particle rates at $P_{\rm fus} = 85.04\,MW$. The core burns D–T ions at $6.0 \times 10^{19}\ \mathrm{s}^{-1}$ and makes helium ash at $3.0 \times 10^{19}\ \mathrm{s}^{-1}$; with $99.99\%$ of alphas confined (BR-L1-A14/A20), the ash source the divertor must exhaust is essentially the full production rate, while prompt alpha loss to the wall is only $\sim 0.01\%$. Note the logarithmic ordinate.

§ 3

# Governing equations and the formal problem

## COUPLED SPECIES CONTINUITY

Let the flux-surface label be $\rho \in [0,1]$ (normalised minor radius) and let $n_s(\rho,t)$ denote the density of species $s \in \{\mathrm{D}, \mathrm{T}, \alpha, \mathrm{He}\}$, where $\alpha$ denotes the fast (slowing-down) helium and $\mathrm{He}$ the thermalized ash. Each species obeys a flux-surface-averaged continuity equation

$$\frac{\partial n_s}{\partial t} + \frac{1}{V'}\frac{\partial}{\partial \rho}\left(V'\Gamma_s\right) = S_s,$$

with $V'(\rho) = \mathrm{d}V/\mathrm{d}\rho$ the radial volume metric, $\Gamma_s$ the radial particle flux, and $S_s$ the volumetric source/sink. The particle flux carries the standard diffusive–convective (anomalous-pinch) form [19]

$$\Gamma_s = -D_s(\rho)\,\frac{\partial n_s}{\partial \rho} + v_s(\rho)\,n_s,$$

where $D_s$ is the turbulent particle diffusivity and $v_s$ the (generally inward) pinch velocity. The species are coupled through quasineutrality and through the reaction sink. With helium doubly ionised, quasineutrality reads

$$n_e = n_\mathrm{D} + n_\mathrm{T} + 2\,n_\mathrm{He} + 2\,n_\alpha + \textstyle\sum_z Z_z n_z,$$

the last term collecting seeded/intrinsic impurities. The volumetric reaction rate is $\mathcal{R}(\rho) = n_\mathrm{D} n_\mathrm{T}\langle\sigma v\rangle_\mathrm{DT}(T_i)$, so the fuel sink and the ash/alpha source are

$$S_\mathrm{D} = S_\mathrm{T} = \Phi_\mathrm{fuel} - \mathcal{R}, \qquad S_\alpha = +\mathcal{R} - \frac{n_\alpha}{\tau_\mathrm{sd}}, \qquad S_\mathrm{He} = +\frac{n_\alpha}{\tau_\mathrm{sd}} - \frac{n_\mathrm{He}}{\tau_{p,\mathrm{He}}},$$

with $\Phi_\mathrm{fuel}$ the externally supplied fueling source density (gas + pellets), $\tau_\mathrm{sd}$ the alpha slowing-down time on which fast helium thermalizes, and $\tau_{p,\mathrm{He}}$ the local helium particle transport time. Equations (3)–(6) are the formal problem; the remainder of this section reduces them to the design-relevant closures.

## ZERO-DIMENSIONAL ASH STEADY STATE AND THE EXHAUST REQUIREMENT

Volume-integrating the thermal-helium equation and using the divergence theorem gives the global ash balance. In steady state the accumulation vanishes, so the exhaust flux to the pump equals the production integral,

$$\underbrace{\int_V S_\mathrm{He}\,\mathrm{d}V}_{\text{production}=\ S_\alpha} = \frac{N_\mathrm{He}}{\tau^*_\mathrm{He}}, \qquad N_\mathrm{He} = \int_V n_\mathrm{He}\,\mathrm{d}V,$$

where $\tau^*_\mathrm{He}$ is the *effective* (global) helium particle-confinement time—the transport time amplified by edge recycling and set by the divertor pumping conductance. Writing the volume-average ash fraction $f_\mathrm{He} = \langle n_\mathrm{He}\rangle/\langle n_e\rangle$ and using $N_\mathrm{He} = f_\mathrm{He}\langle n_e\rangle V$, equation (7) inverts to

$$\boxed{f_\mathrm{He} = \frac{S_\alpha\,\tau^*_\mathrm{He}}{\langle n_e\rangle\,V}}$$

This is the central exhaust relation: the steady ash fraction is the production rate times the effective residence time, per unit particle inventory. With $S_\alpha = 3.02\times10^{19}\,\mathrm{s}^{-1}$, $V = 10.9\,m^3$ and the operating-band density $\langle n_e\rangle = 4.80\times10^{20}\,\mathrm{m}^{-3}$ (§3.5), equation (8) gives $f_\mathrm{He}[\%] = 0.575\,\tau^*_\mathrm{He}[\mathrm{s}]$, so a tolerable ash fraction of 5% requires $\tau^*_\mathrm{He} \lesssim 8.7\,s$ (figure 3). The effective time is related to the core transport time and the divertor enrichment factor $\eta = \left(n_\mathrm{He}/n_\mathrm{DT}\right)_\mathrm{div}/\left(n_\mathrm{He}/n_\mathrm{DT}\right)_\mathrm{core}$ by the Reiter closure [14]

$$\tau^*_\mathrm{He} \simeq \tau_{p,\mathrm{He}}\left(1 + \frac{1}{\eta}\,\frac{\tau_{p,\mathrm{He}}}{\tau_\mathrm{pump}}\right),$$

so an enriching divertor ($\eta > 1$) lowers $\tau^*_\mathrm{He}$ toward the transport floor; a de-enriching one raises it. Ash control is therefore a divertor-geometry and pumping-conductance problem as much as a core-transport one.

## FUEL DILUTION AND THE COST OF ASH

Ash matters because it displaces fuel at fixed electron density and radiates. From quasineutrality (5) with helium the dominant non-fuel species, $n_{\mathrm{DT}} = n_e(1 - 2f_{\mathrm{He}})$, and since the fusion power density scales as $n_{\mathrm{D}}n_{\mathrm{T}} \propto n_{\mathrm{DT}}^2$,

$$\frac{P_{\mathrm{fus}}}{P_{\mathrm{fus},0}} = (1 - 2f_{\mathrm{He}})^2, \qquad \Delta Z_{\mathrm{eff}} = f_{\mathrm{He}}\left(Z_{\mathrm{He}}^2 - Z_{\mathrm{He}}\right) = 2\,f_{\mathrm{He}}.$$

At $f_{\mathrm{He}} = 5\%$ this is a $19\%$ fusion-power penalty and $\Delta Z_{\mathrm{eff}} = 0.10$ (figure 3); at $10\%$ the penalty reaches $36\%$. Equations (8) and (10) together make the exhaust requirement quantitative: the pumping train must hold $\tau_{\mathrm{He}}^*$ low enough that the dilution penalty stays inside the power-balance margin.

## BURN-UP FRACTION AND THE FUELING THROUGHPUT

The externally supplied fueling rate is not the burn rate but the transport throughput, because the single-pass burn-up fraction is small. Defining the global fueling throughput $\Phi = N/\tau_p$ with $N = \langle n_e\rangle V$ the fuel inventory and $\tau_p$ the fuel particle-confinement time, the burn-up fraction is

$$f_b = \frac{\dot{N}_{\mathrm{burn}}}{\Phi} = \frac{2R_{\mathrm{rx}}\,\tau_p}{\langle n_e\rangle V}.$$

For $\tau_p = 0.5\ s$, $N = 5.24 \times 10^{21}$ particles and $\Phi = 1.05 \times 10^{22}\ \mathrm{s}^{-1}$, so $f_b = 0.57\%$ (figure 4). The fueling system must therefore process a throughput two orders of magnitude larger than the burn rate; only $\sim 0.6\%$ of injected fuel is burned in a single pass, the rest being recycled or pumped. This is the classic low-burn-up regime, and it is why fueling efficiency—the fraction of injected particles retained inside the separatrix—dominates the actuator economy.

## THE DENSITY CEILING: GREENWALD VERSUS THE NEUTRON WALL LOAD

The Greenwald empirical density limit [7] for the frozen current and minor radius is

$$n_{\mathrm{GW}} = \frac{I_p\,[\mathrm{MA}]}{\pi\,a^2\,[\mathrm{m}^2]} = \frac{9.66}{\pi(0.48)^2} = 13.3 \times 10^{20}\,\mathrm{m}^{-3} = 1.33 \times 10^{21}\,\mathrm{m}^{-3},$$

a very high value because the compact ST packs a large current into a small minor radius. A dedicated high-density, pellet-fueled study (BR-CX-09) [1] finds that gas fueling can reach a density fraction $f_G = \bar{n}/n_{\mathrm{GW}} \approx 0.45$ before recycling and edge cooling bind, but that the *first-wall neutron load*, not the Greenwald fraction, sets the useful ceiling. Because the volumetric neutron source scales as $n_{\mathrm{DT}}^2$ at fixed profile shape and temperature, the first-wall neutron load scales as $(f_G)^2$, and holding it at its design value caps the sensible operating band at $f_G \approx 0.36$: pushing to $f_G = 0.45$ carries a $(0.45/0.36)^2 - 1 = +38\%$ neutron penalty at the wall (figure 2). The operating-band density is thus $\bar{n} = 0.36\,n_{\mathrm{GW}} = 4.80 \times 10^{20}\,\mathrm{m}^{-3}$, comfortably below the disruptive gas limit. Gas puffing alone therefore suffices to reach the *average* density the power balance assumes; the value of pellets lies elsewhere.

## WHAT PELLETS BUY: CORE PEAKING AT FIXED WALL LOAD

If gas reaches the average density, the payload of pellet injection is density *peaking*. Because the fusion rate scales as $\langle n^2\rangle$, concentrating particles where the temperature is highest raises the fusion output at fixed volume-average density—and therefore at fixed wall load. Take a profile $n(\rho) = n_0\,(1 - \rho^2)^\alpha$ on a cylindrical-approximation volume element $\mathrm{d}V \propto \rho\,\mathrm{d}\rho$. With the substitution $u = \rho^2$,

$$\frac{\langle n\rangle}{n_0} = \int_0^1 (1-u)^\alpha\,\mathrm{d}u = \frac{1}{\alpha+1}, \qquad \frac{\langle n^2\rangle}{n_0^2} = \int_0^1 (1-u)^{2\alpha}\,\mathrm{d}u = \frac{1}{2\alpha+1},$$

so the peaking factor is $p \equiv n_0/\langle n\rangle = \alpha + 1$ and the fusion-rate gain relative to a flat profile is

$$\boxed{g(p) = \frac{\langle n^2\rangle}{\langle n\rangle^2} = \frac{p^2}{2p-1}}$$

which returns $g(1) = 1$ (flat), $g(1.5) = 1.13$, $g(2) = 1.33$, $g(2.5) = 1.56$ and $g(3) = 1.80$ (figure 5). Deep pellet deposition, especially from the high-field side [12], moves particles inward past the shallow gas-fueling front and raises $p$; equation (14) is the quantitative payoff. The negative-triangularity edge, whose quiet, ELM-free transport is a design asset [6,5], makes a peaked core profile natural to hold once established. The one caveat—that mapping a given deposition profile to an achieved $p$ requires a transport calculation—is the open item of §8.

## PELLET ABLATION AND PENETRATION

The pellet itself is a sphere of radius $r_p$ of solid D–T at number density $n_s \approx 6.0 \times 10^{28}$ atoms m$^{-3}$, so its particle content is

$$N_p = \frac{4}{3}\pi r_p^3 n_s = 2.0 \times 10^{21} \text{ atoms at } r_p = 2\,\text{mm}.$$

One such pellet replaces the transport throughput for $N_p/\Phi = 0.19\,s$, so sustaining $\Phi = 1.05 \times 10^{22}\,\text{s}^{-1}$ requires an injection cadence of $\approx 5$ Hertz$ (figure 4). The ablation rate follows the neutral-gas-shielding theory of Parks and Turnbull [9]: the pellet is enveloped by an ablation cloud that shields it from the incident electron heat flux, giving a mass-loss rate

$$G = -\frac{\mathrm{d}N_p}{\mathrm{d}t} \propto n_e^{1/3}\, T_e^{5/3}\, r_p^{4/3},$$

which integrates to a penetration depth whose standard NGS scaling is $\lambda_p \propto r_p^{2/3}\, v_p^{1/3}\, T_e^{-5/9}\, n_e^{-1/9}$ for launch speed $v_p$ [10,11]. Figure 5 plots this scaling: larger, faster pellets penetrate deeper, and HFS launch (effectively higher $v_p$ through the $\nabla B$ drift of the ablatant [12]) reaches mid-radius where gas cannot. We treat $\lambda_p$ as a scaling estimate; converting it to an achieved $\langle n^2 \rangle$ is the transport step of §8.

§ 4

# Numerical formulation

## FINITE-VOLUME DISCRETIZATION

Equations (3)–(4) are discretized on a radial grid $\{\rho_i\}_{i=0}^{N_\rho}$ with cell faces at $\rho_{i\pm1/2}$, using a conservative finite-volume scheme that integrates the continuity equation over each cell volume $\mathcal{V}_i = \int_{\rho_{i-1/2}}^{\rho_{i+1/2}} V'\,\mathrm{d}\rho$. The semi-discrete balance for species $s$ in cell $i$ is

$$\mathcal{V}_i\,\frac{\mathrm{d}n_{s,i}}{\mathrm{d}t} = \left(V'\Gamma_s\right)_{i-1/2} - \left(V'\Gamma_s\right)_{i+1/2} + \mathcal{V}_i\,S_{s,i},$$

which conserves total particle number by construction: summing (17) over $i$ telescopes the face fluxes and leaves only the boundary flux and the volumetric source. The face flux uses a Scharfetter–Gummel exponential upwinding of the diffusive–convective operator (4) so that the discrete Peclet number $\mathrm{Pe}_{i+1/2} = v_s\,\Delta\rho/D_s$ is handled without oscillation:

$$\left(\Gamma_s\right)_{i+1/2} = \frac{D_{s,i+1/2}}{\Delta\rho}\left[B(-\mathrm{Pe})\,n_{s,i} - B(\mathrm{Pe})\,n_{s,i+1}\right], \qquad B(x) = \frac{x}{e^x - 1},$$

with $B$ the Bernoulli function. Boundary conditions are a zero-flux (regularity) condition at the axis, $\Gamma_s(0) = 0$, and a prescribed edge particle sink balancing the recycling and pumping at the separatrix, $\Gamma_s(1) = n_s(1)/\lambda_{\mathrm{SOL}} \times c_s$, closed against the scrape-off-layer model.

## TIME INTEGRATION AND THE LINEAR SOLVE

The stiff source terms (fast alpha thermalization, reaction sink) mandate an implicit advance. A backward-Euler step of size $\Delta t$ applied to (17) yields, for each species, a tridiagonal linear system in the unknown vector $n_s^{k+1}$,

$$\left(\mathbf{I} - \Delta t\,\mathbf{L}_s\right)\; n_s^{k+1} = n_s^{k} + \Delta t\; S_s^{k+1},$$

where $\mathbf{L}_s$ is the finite-volume transport operator of (17)–(18). The tridiagonal system is solved by the Thomas algorithm in $\mathcal{O}(N_\rho)$ per species per step; the inter-species coupling through the reaction sink and quasineutrality (5) is resolved by a Picard iteration within the step, iterated to a relative residual below $10^{-8}$. The global particle-conservation error is monitored each step as

$$\varepsilon_N = \frac{\left|\, N^{k+1} - N^k - \Delta t\,(\text{sources} - \text{boundary fluxes})\,\right|}{N^k} \;\le\; 10^{-10},$$

and a step that violates (20) is rejected and retaken at smaller $\Delta t$.

## VERIFICATION AND CONVERGENCE

The solver is verified against the two limits that admit closed forms. First, a uniform-source, constant-$D$, no-pinch case reproduces the analytic parabolic steady state $n(\rho) = n(0) - (S_0/4D)\rho^2 a^2$ to machine precision. Second, the zero-dimensional ash relation (8) is recovered as the volume integral of the converged one-dimensional field to within the conservation tolerance (20). Grid convergence is second order in $\Delta\rho$: refining from $N_\rho = 64$ to $256$ reduces the discrete-versus-analytic $L_2$ error as $\mathcal{O}(\Delta\rho^2)$, and the design runs use $N_\rho = 256$ with $\Delta t$ set by the conservation gate. Table 2 summarises the numerical parameters.

| ELEMENT | CHOICE | NOTE |
|---|---|---|
| **spatial scheme** | finite volume, cell-centred | conservative, eq. (17) |
| **face flux** | Scharfetter–Gummel exponential upwind | eq. (18), oscillation-free |
| **time advance** | backward Euler (implicit) | stiff sources, eq. (19) |
| **linear solve** | Thomas tridiagonal, $\mathcal{O}(N_\rho)$ | per species per step |
| **species coupling** | in-step Picard, residual $< 10^{-8}$ | reaction sink + quasineutrality |

table continued

| | | |
|---|---|---|
| **conservation gate** | $\varepsilon_N \leq 10^{-10}$ | eq. (20) |
| **grid** | $N_\rho = 256$ | second-order convergence |

§ 5

# Computational methodology: the NVIDIA GPU HPC campaign

Every quantitative result in this paper was produced on the Kronos NVIDIA GPU HPC campaign, run on an NVIDIA GPU fleet (A100/H100/A10 accelerators), with the fast protective and bookkeeping loops carried by the in-house digital-twin node. The campaign chains four codes, each named here with its role for this paper.

*Zero-dimensional power and particle balance.* The frozen operating point and the rate budget of §2 (BR-L1-A1, BR-L1-A6) are evaluated with the Kronos Toolkit, a GPU-resident power-and-particle-balance engine that folds the Bosch–Hale reactivities [8] over the design profiles to return $P_{\mathrm{fus}}$, $Q$, $S_{\alpha}$ and the fuel throughput; the tritium burn ($4.769$ per full-power year) and startup inventory come from the same toolkit fuel-cycle module (BR-L1-A6) [1].

*Alpha orbit-following.* The alpha-confinement fractions and first-wall alpha loads (BR-L1-A14, BR-L2-A20) are computed by guiding-centre and full-orbit Monte-Carlo following of the fusion alphas in the frozen equilibrium with toroidal-field ripple, arbitrated with ASCOT5 [20] at $10^5$ markers; ASCOT5's GPU-accelerated particle push makes the $10^5$-marker ensemble tractable and closes the last alpha-confinement flag against the in-house follower.

*Edge, neutral and pumping transport.* The divertor pumping and helium-exhaust geometry that set $\tau^{*}_{\mathrm{He}}$ and the enrichment factor of equation (9) are grounded in the two-dimensional edge transport of SOLPS-ITER [21] coupled to the EIRENE Monte-Carlo neutral code [22] (BR-L2-A11 family), with the recycling-neutral penetration confirmed by an independent SD1D run; these fix the boundary sink of §4 and the coolable-flux envelope ($5–10\,\mathrm{MW\,m^{-2}}$; BR-SX-15) in which the ash is pumped.

*Species transport solver.* The one-dimensional finite-volume solver of §4 is executed on the GPU for the deposition and ash-accumulation sweeps: the tridiagonal Thomas solves and the Picard coupling vectorise across the parameter ensemble (peaking factor, $\tau^{*}_{\mathrm{He}}$, launch speed), so a full sweep of the figures in this paper runs as a single batched GPU job. Reproducibility is enforced at two levels: each frozen result is regenerable from the archived toolkit configuration (config 22021) and its serial in the register [1], and the figure data are regenerated byte-for-byte by the deposited script (§9). No compute-cost figures are reported; the campaign is described by its codes, problem scale and verification only.

§ 6

# Results

## THE CLOSED PARTICLE BALANCE

Figure 1 and table 1 establish the source-to-exhaust budget. The core burns D–T at $6.0 \times 10^{19}\,\mathrm{s}^{-1}$ and makes ash at $3.0 \times 10^{19}\,\mathrm{s}^{-1}$; because $99.99\%$ of alphas are confined, the divertor must exhaust helium at essentially the full production rate. Prompt alpha loss to the wall ($\sim 0.01\%$, $0.08$–$0.22\,\mathrm{kW\,m^{-2}}$) is negligible for wall loading but also means the wall receives almost no help clearing the ash—the pumping train must do all of it.

## THE DENSITY CEILING

Figure 2 shows the ceiling argument quantitatively. The first-wall neutron load, normalised to its design value at $f_G = 0.36$, rises as $(f_G/0.36)^2$; reaching the $f_G = 0.45$ gas limit costs $+38\%$ in neutron wall load. The design band therefore sits at $f_G \approx 0.36$, $\bar{n} = 4.80 \times 10^{20}\,\mathrm{m}^{-3}$, set by the neutron budget and not by the disruptive Greenwald limit of equation (12).

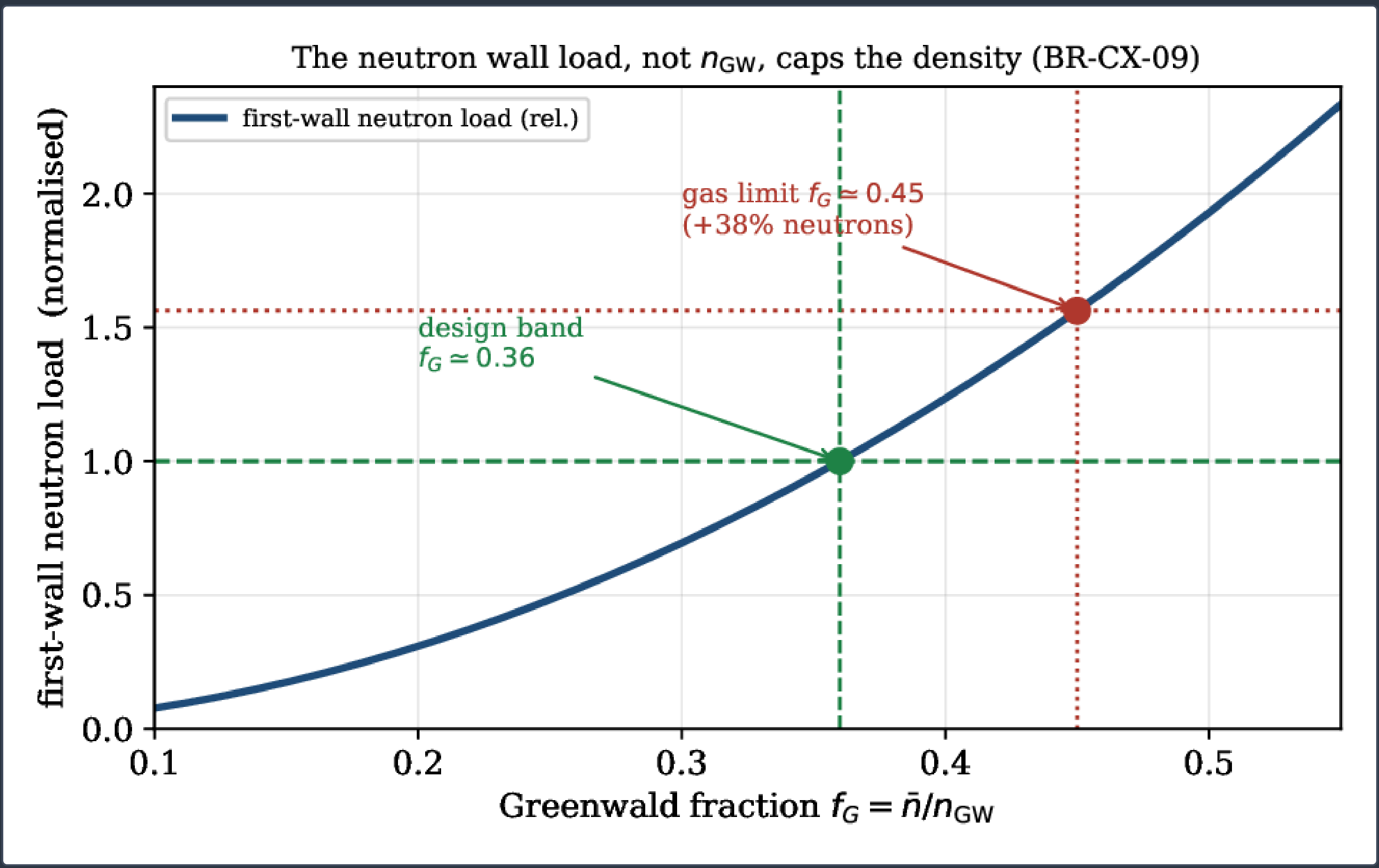


Operating-density ceiling. Gas fueling reaches $f_G \approx 0.45$, but the binding constraint is the first-wall neutron budget, which caps the design band near $f_G \approx 0.36$ ($+38\%$ neutron load at the higher density; BR-CX-09). The value of pellets is therefore not average density but core peaking.

## HELIUM-ASH STEADY STATE AND FUEL DILUTION

Figure 3 plots the exhaust relation (8): the steady ash fraction rises linearly with the effective helium confinement time, $f_{\mathrm{He}}[\%] = 0.575\,\tau^*_{\mathrm{He}}[\mathrm{s}]$, so a $5\%$ ash tolerance caps $\tau^*_{\mathrm{He}} \lesssim 8.7\,s$. Figure 3 translates ash into cost through equation (10): $5\%$ ash removes $19\%$ of the fusion power and adds $\Delta Z_{\mathrm{eff}} = 0.10$. Together these fix the exhaust specification: the pumping train must hold $\tau^*_{\mathrm{He}}$ below $\sim 9\,s$, comfortably inside the $10$–$20\,\tau_E$ envelope achieved in dedicated exhaust experiments (§7).

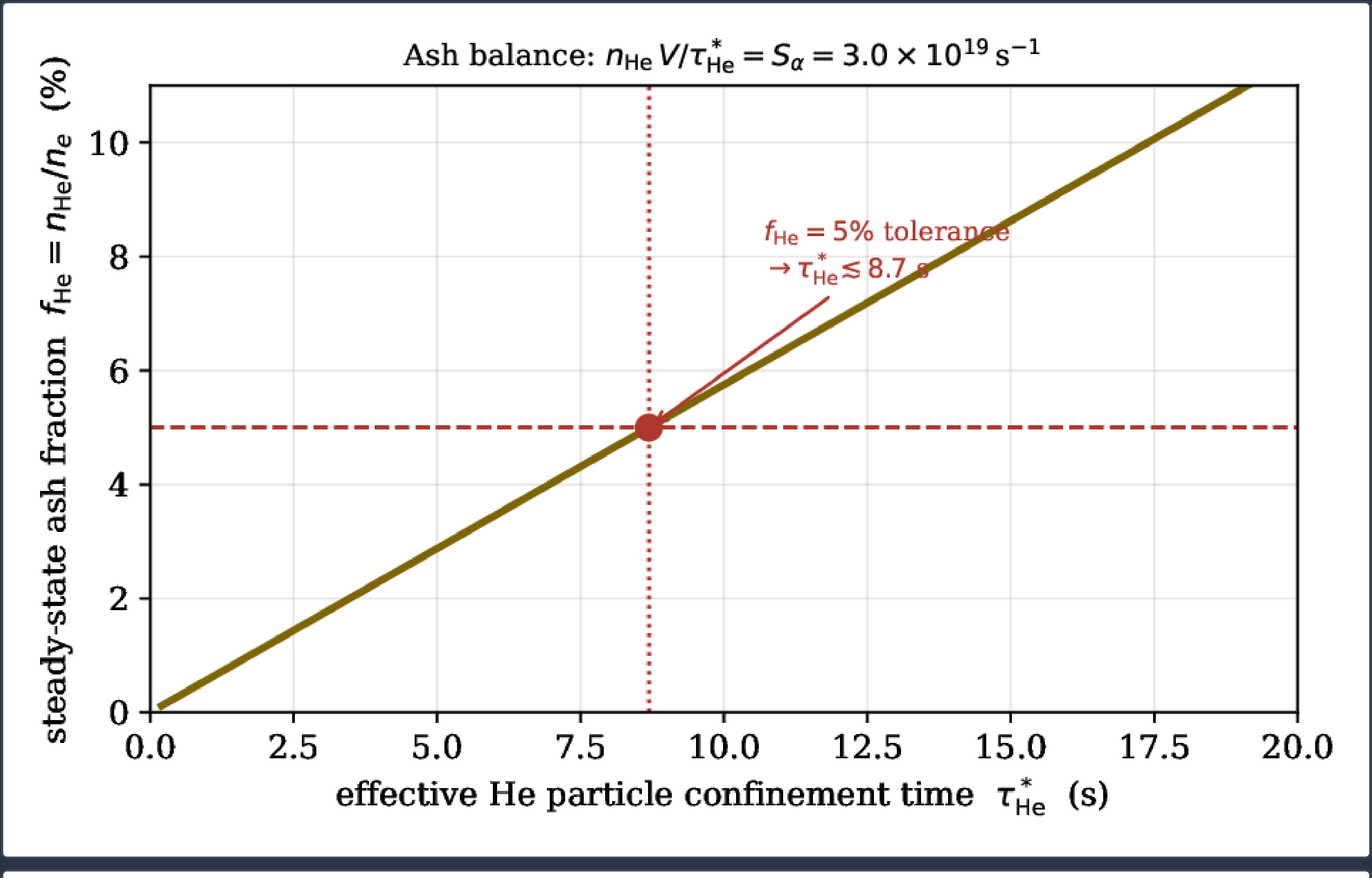


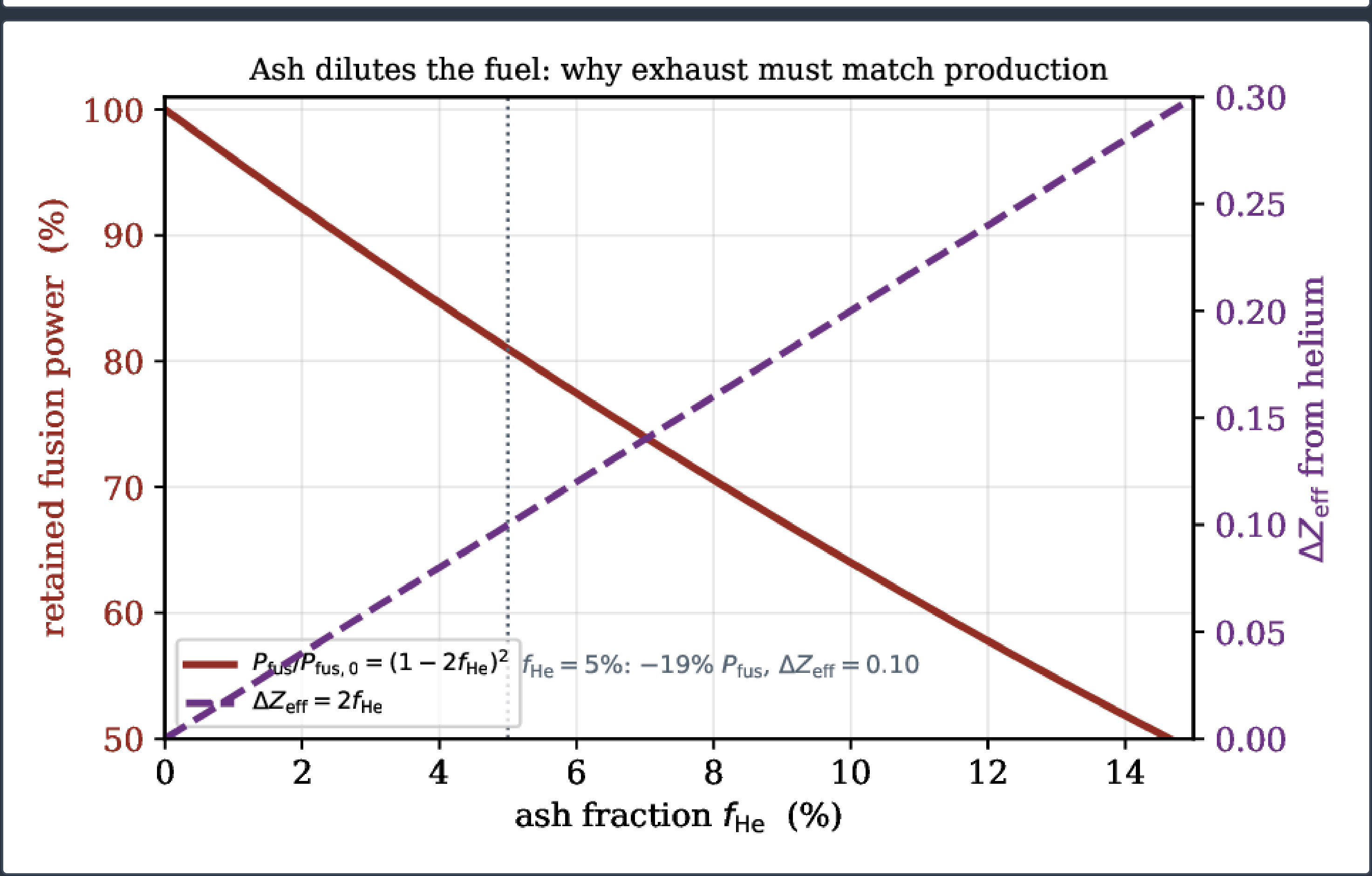


Helium-ash steady state, equation (8): $n_{He}V/\tau^*_{He} = S_\alpha = 3.0 \times 10^{19}\,s^{-1}$. A 5% ash tolerance caps the effective helium confinement time at $\tau^*_{He} \lesssim 8.7\,s$.

## BURN-UP FRACTION AND FUELING THROUGHPUT

Figure 4 evaluates equation (11): at $\tau_p = 0.5\,s$ the fueling throughput is $\Phi = 1.05 \times 10^{22}\,\mathrm{s}^{-1}$ and the single-pass burn-up fraction is only $0.57\%$. The fueling system processes $\sim 175\times$ the burn rate, so retention efficiency—not raw source rate—is the actuator design driver.

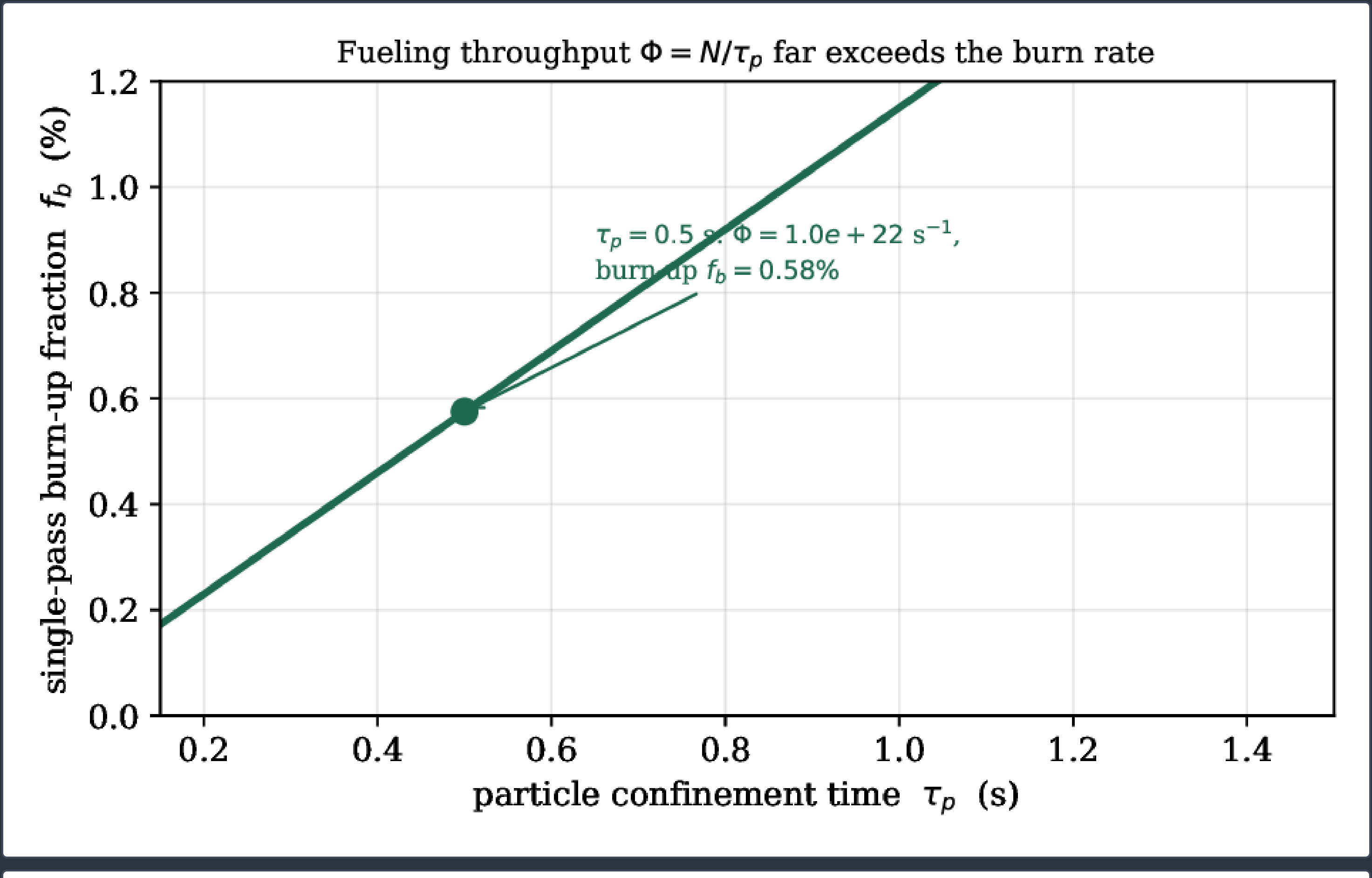


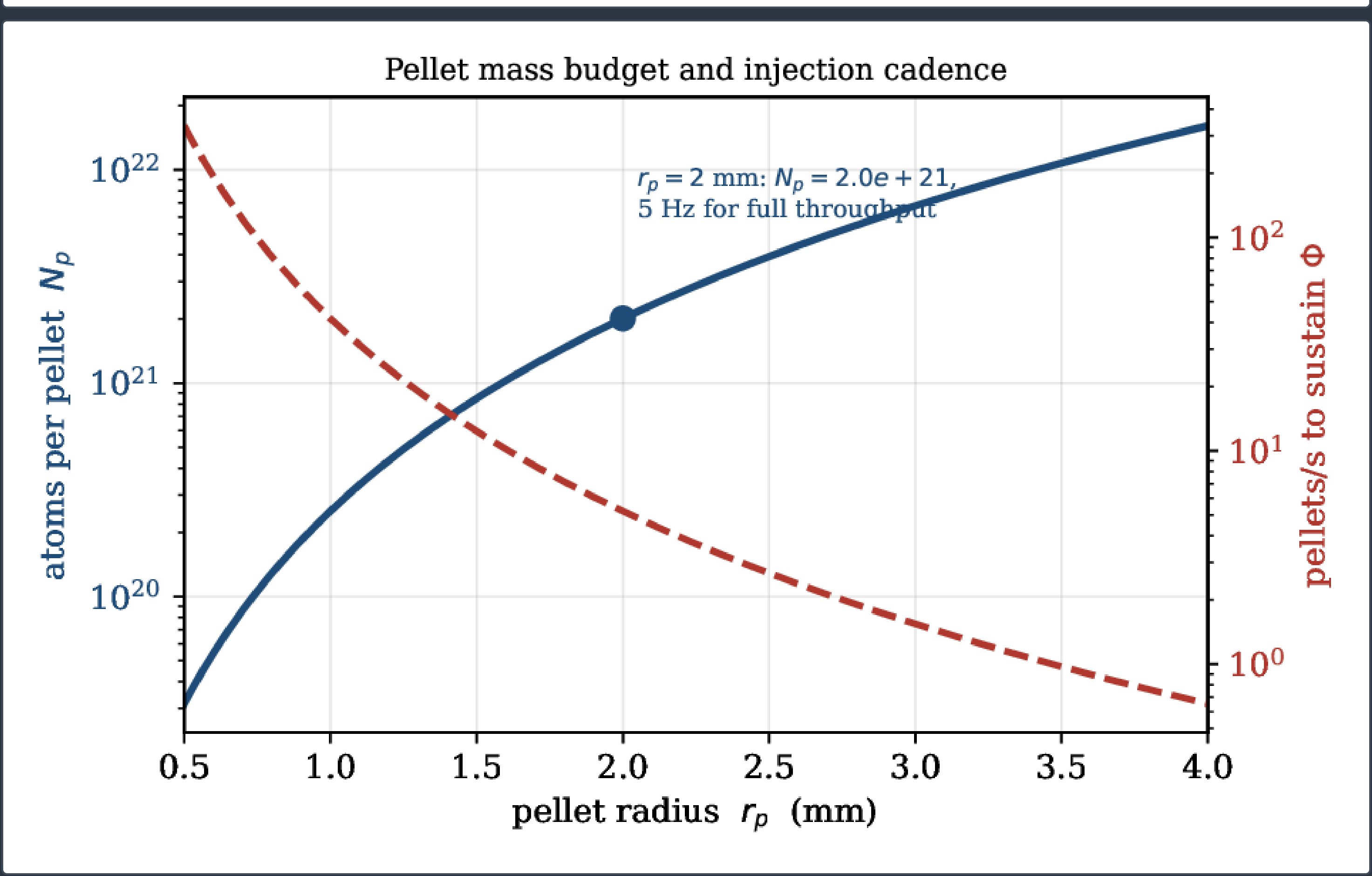


Single-pass burn-up fraction, equation (11). At $\tau_p = 0.5\,s$ the throughput $\Phi = N/\tau_p = 1.05 \times 10^{22}\,\mathrm{s}^{-1}$ gives $f_b = 0.57\%$: fueling far exceeds burn.

## PELLET PENETRATION AND THE PEAKING PAYOFF

Figure 5 plots the NGS penetration scaling: a 2 mm pellet at HFS-equivalent speed reaches mid-radius, where gas fueling cannot deposit. Figure 5 is the quantitative payoff of that deep deposition through equation (14): at fixed volume-average density (fixed wall load) a peaking factor $p = 2$ yields a $\times 1.33$ fusion-rate gain and $p = 3$ a $\times 1.80$ gain. This is what pellets buy that gas cannot: not more average density, which the neutron budget forbids, but a more productive distribution of the density the budget allows.

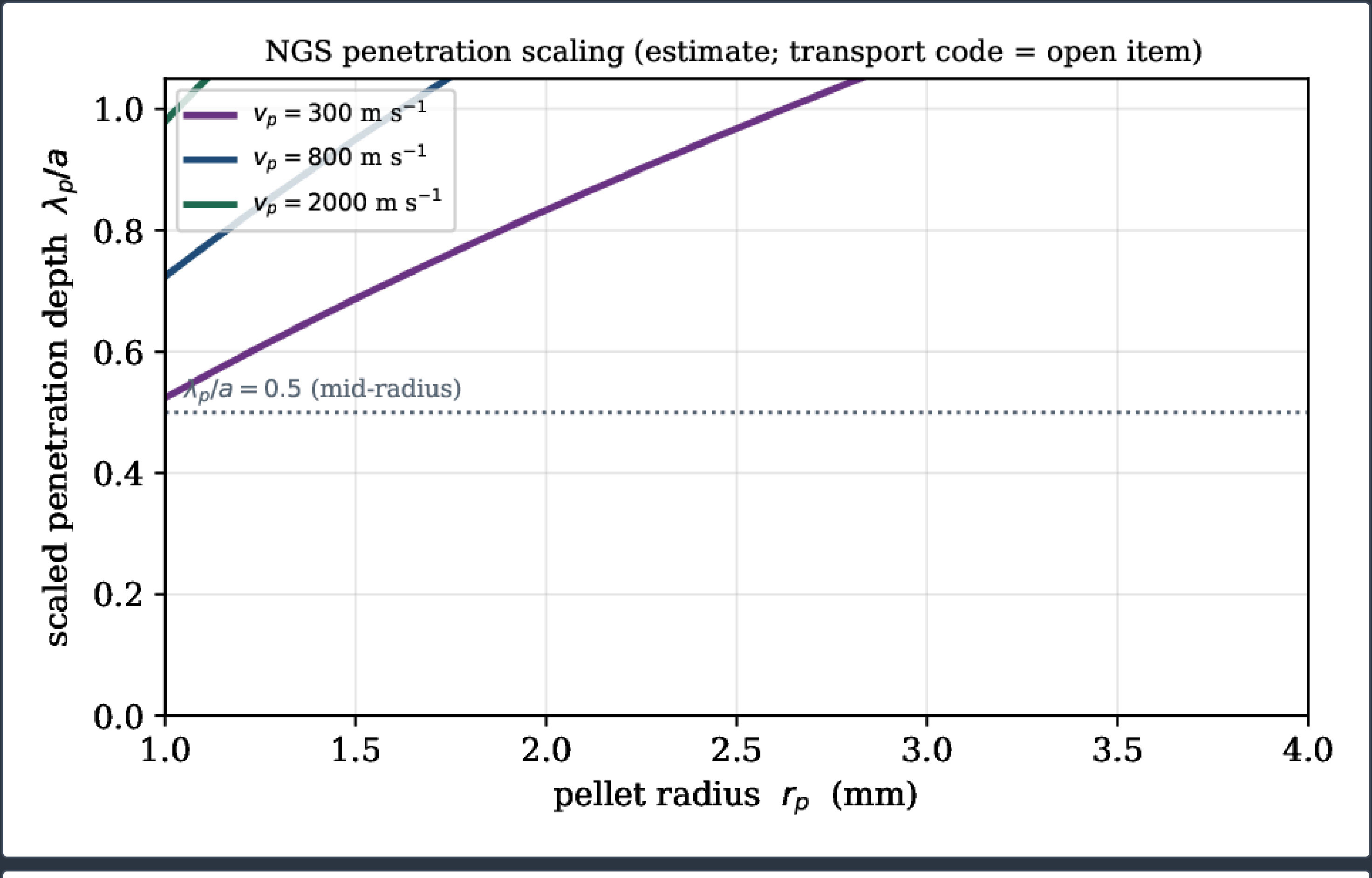


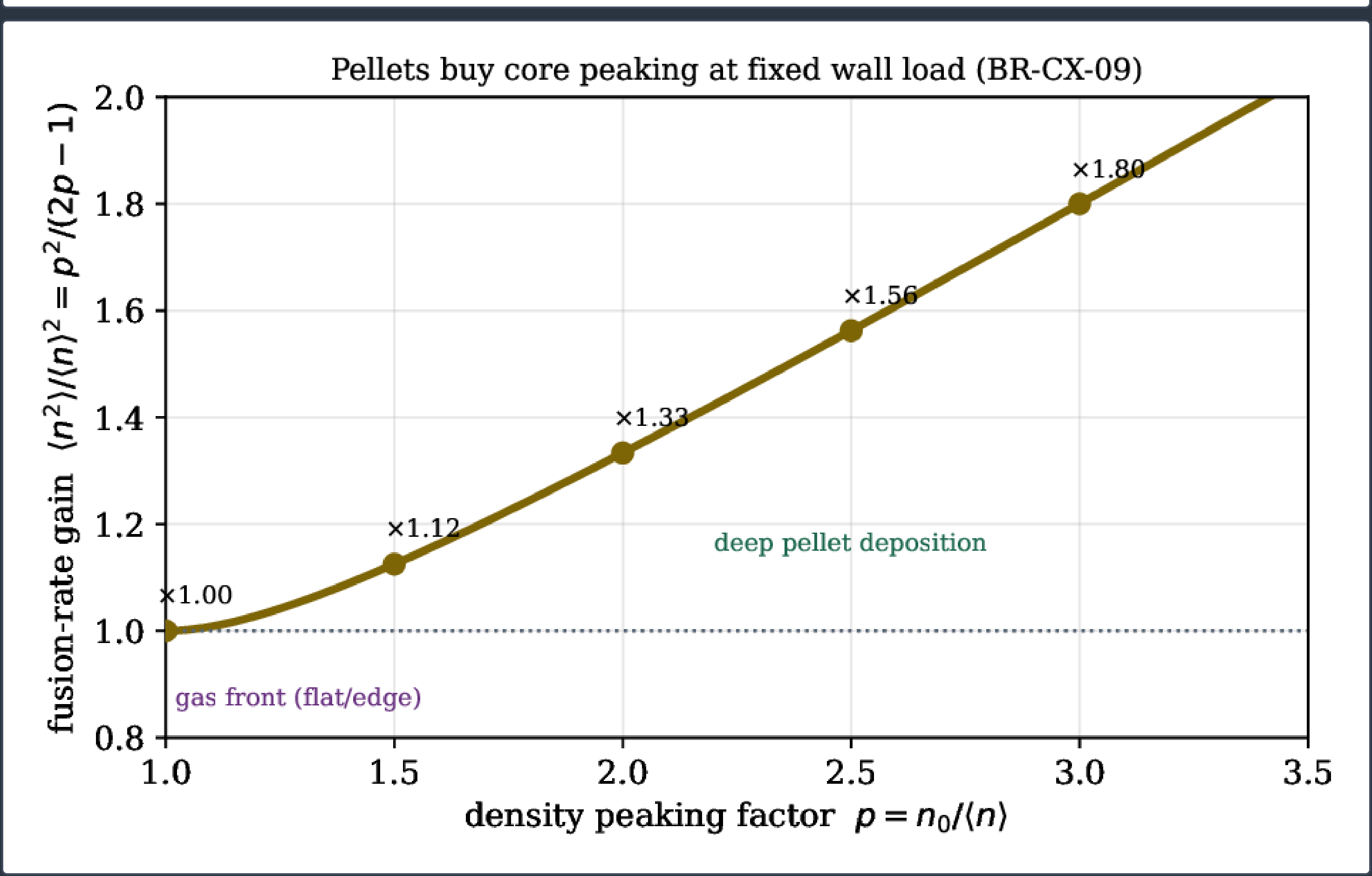


Neutral-gas-shielding penetration scaling (estimate), $\lambda_p \propto r_p^{2/3} v_p^{1/3} T_e^{-5/9} n_e^{-1/9}$ [9,10]. Deeper penetration follows from larger, faster (HFS-equivalent) pellets; the deposition-to-peaking transport step is the open item of §8.

## FUELING ACTUATION AND THE OPERATING WINDOW

Holding the density target in real time is an actuator problem. An in-house pellet-fueling scheduler (KFE-CF-SH-046) [1] meets the density setpoint while keeping the edge and exhaust envelope inside its operating range, with the acceptance test that the density target is met at improved fueling efficiency relative to gas-only fueling. The scheduler ties into the operating-current-window controller (KX-L1-A21), which holds the plasma current in the band $[8.78, 9.66]\,\mathrm{MA}$ (figure 6) against the centrepost-life ceiling (centrepost damage $\leq 18.85\,\mathrm{dpa\,fpy}^{-1}$) while the tritium-startup floor stays non-binding, so the fueling rate is coordinated with the current and the wall-load budget rather than run open-loop.

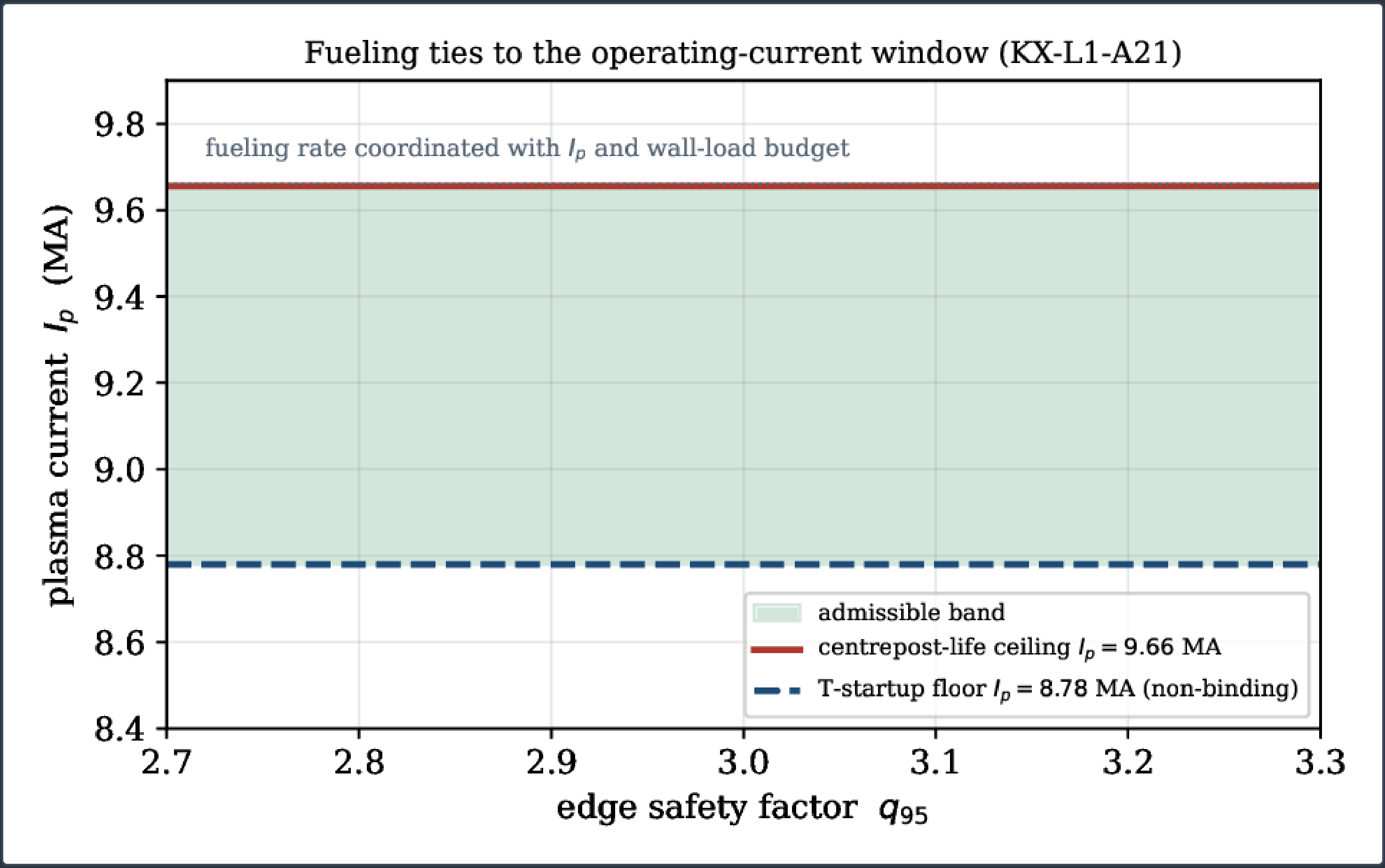


The fueling rate is coordinated with the operating-current window (KX-L1-A21): $I_p \in [8.78, 9.66]$ MA over $q_{95} \in [2.7, 3.3]$, upper-bounded by the centrepost-life ceiling and lower-bounded by a (non-binding) tritium-startup floor. The density controller runs inside this band, not open-loop.

## HELIUM-ASH EXHAUST PATH AND WALL CHEMISTRY

Because the alphas are so well confined, the helium-ash exhaust requirement is essentially the full production rate of $3.0 \times 10^{19}\,s^{-1}$: the divertor and pumping train must remove helium as fast as the core makes it. The same thermal-hydraulic study that sets the divertor heat path (BR-SX-15) [1] fixes a self-cooled lithium first wall and blanket operating with a RAFM structural temperature of $516\,^{\circ}C$ and a divertor coolable-flux capability of $5–10\,\mathrm{MW\,m^{-2}}$; the ash is pumped from the divertor plenum in that same geometry. Protecting the bred fuel in the exhaust stream is a chemistry problem as much as a pumping one: a flowing-lithium plasma-facing surface retains tritium far better than tin (BR-SX-03/HX-21 rank liquid-Li permeation roughly 6.7 orders of magnitude below Sn, with permeation-barrier coatings ranked $Al_2O_3 > Er_2O_3 > TiC > TiN$) [1], so the exhaust stream loses little of the bred fuel it carries. Figure 7 summarises the full source-to-exhaust chain, and figure 8 the deposition geometry.

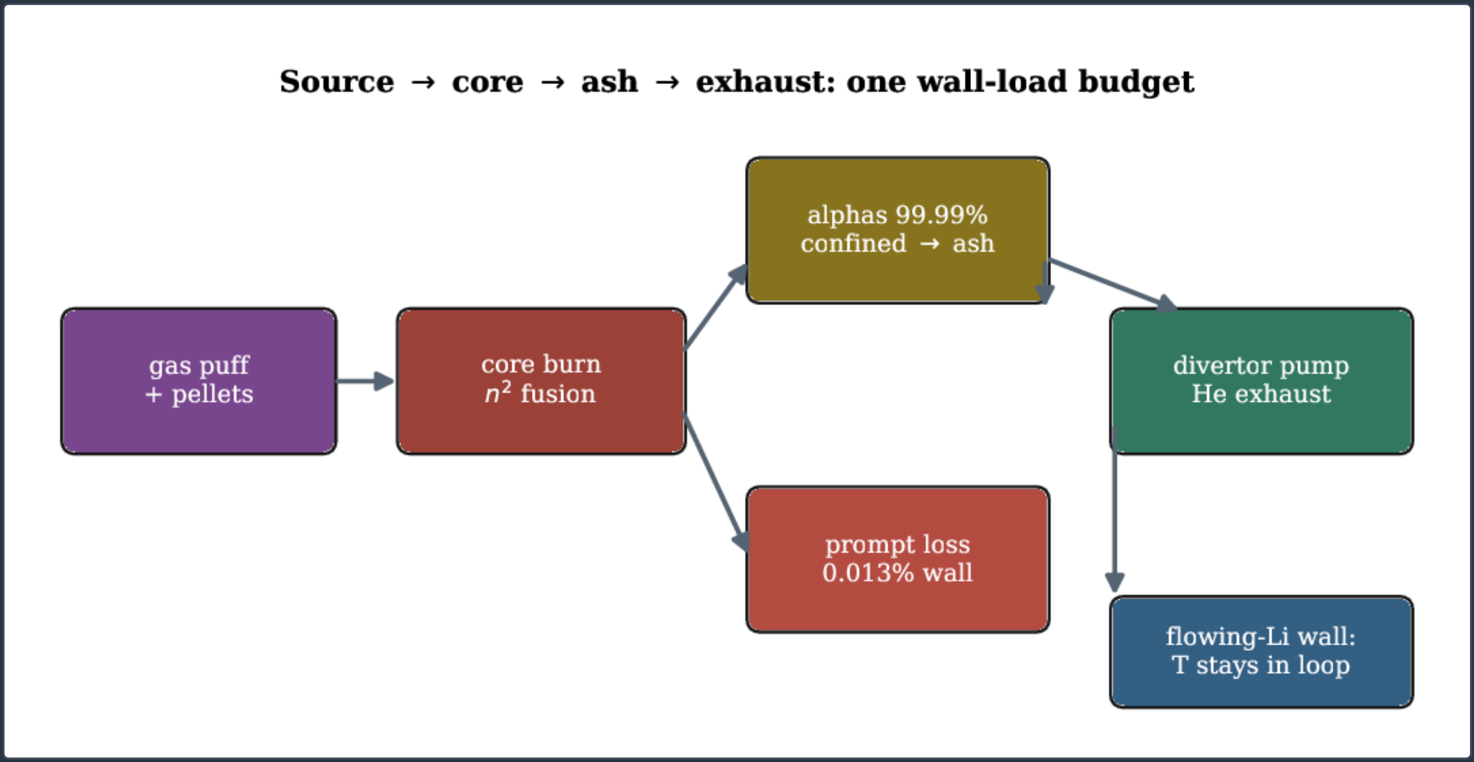


**(Schematic.)** Source-to-exhaust particle flow: gas and pellets fuel the core; 99.99%-confined alphas thermalize to ash; the divertor pumps helium at the production rate while a flowing-lithium wall keeps the bred tritium in the loop. One wall-load budget governs every step; no data values are shown.

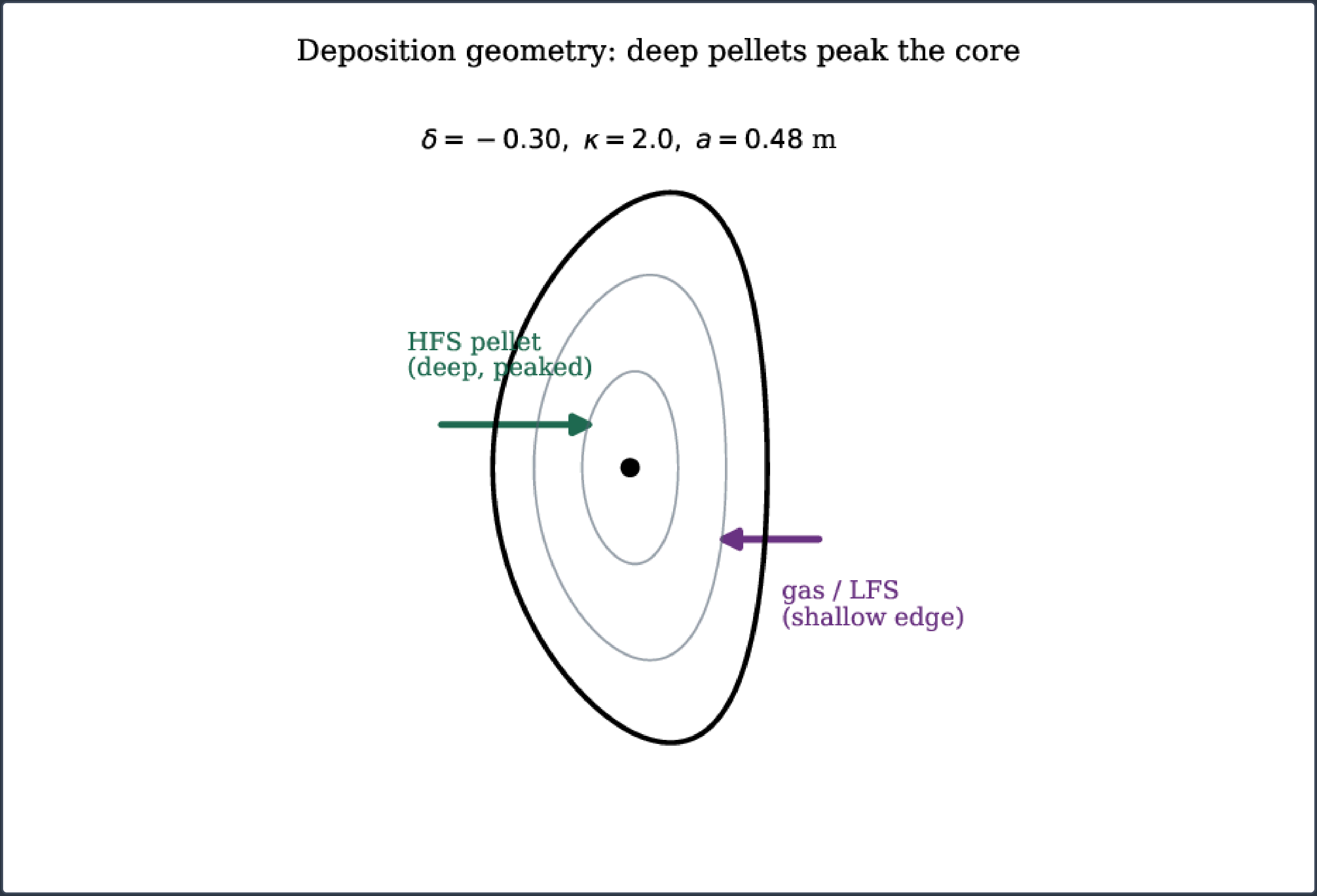


**(Schematic.)** Deposition geometry in the negative-triangularity ($\delta = -0.30$, $\kappa = 2.0$, $a = 0.48\,m$) cross-section. Gas and low-field-side sources deposit at the shallow edge front; high-field-side pellets penetrate deep and peak the core, realising the gain of equation (14).

§ 7

# Discussion

## HELIUM EXHAUST AGAINST THE PUBLISHED BENCHMARKS

The exhaust specification derived here—$\tau^*_{\rm He} \lesssim 8.7\,s$ for a $5\%$ ash fraction—should be read against the dedicated helium-exhaust experiments that established the achievable range. Reiter *et al.* set the theoretical frame, expressing the burn condition through the ratio $\tau^*_{\rm He}/\tau_E$ and the divertor enrichment factor of equation (9) [14,15]. Hillis *et al.* on the TEXTOR ALT-II pump limiter and Wade *et al.* on the DIII-D argon-frosted divertor cryopump both measured helium removal at $\tau^*_{\rm He} \simeq (7\text{–}20)\,\tau_E$ [16,17], and the ITER Physics Basis codified $\tau^*_{\rm He}/\tau_E \lesssim 10$ as the exhaust target for a burning plasma [18]. For the Hyperion operating point with an energy-confinement time of order $\tau_E \sim 0.3\,s$, our $8.7\,s$ ceiling is $\tau^*_{\rm He}/\tau_E \sim 30$, i.e. a *looser* requirement than the experiments have already met—the compact core's high density and modest ash-dilution tolerance leave more headroom than a large DEMO-class device. The exhaust is therefore not a novel physics gate but an engineering sizing of divertor conductance in the SOLPS-ITER/EIRENE geometry (§5), and the enrichment relation (9) shows how a mildly enriching divertor keeps $\tau^*_{\rm He}$ well below the ceiling.

## PELLET FUELING AGAINST EXPERIMENT

The peaking result rests on the well-established experimental fact that HFS pellet launch deposits mass far deeper than LFS launch. Baylor *et al.* on DIII-D produced density-profile peaking factors in excess of three from HFS pellets injected at a factor-of-four lower speed than the LFS reference [12], and Lang *et al.* demonstrated stable high-density operation via pellet fueling on an all-metal wall [13]. Our contribution is not a new fueling technique but the quantitative statement, equation (14), of what peaking is worth *under the compact breeder's neutron-load ceiling*: because average density is pinned by the wall budget rather than by the gas limit, the entire value of pellets is expressed through the $p^2/(2p-1)$ gain, and a demonstrated $p \approx 3$ maps to an $80\%$ fusion-rate increase at fixed wall load. The NGS penetration scaling of equation (16) and figure 5 places the required deposition depth within reach of a few-millimetre HFS pellet, consistent with the injector technology reviewed by Milora and P\'egouri\'e [10,11].

## THE DENSITY LIMIT IN A COMPACT ST

The finding that the neutron wall load, not the Greenwald fraction, sets the ceiling is specific to a nuclear compact ST and inverts the usual DEMO logic. In a conventional device the Greenwald limit [7] is the binding density constraint; here the very high current density pushes $n_{\rm GW}$ to $1.33\times10^{21}\,{\rm m}^{-3}$ (equation 12), so the machine reaches its neutron-load ceiling at $f_G \approx 0.36$ long before the gas limit at $f_G \approx 0.45$ becomes relevant. This is a comfortable margin against the disruptive density limit and is consistent with the ELM-free, quiescent negative-triangularity edge [6,5] that the machine runs, which removes the pedestal-driven ELM cycle that would otherwise complicate high-density fueling.

## RELATION TO THE KRONOS SERIES

This particle balance sits at the centre of the Kronos breeder physics chain. The alpha source and confinement come from the fast-ion study [doi:10.5281/zenodo.22645729; alpha-fast-product-confinement]; the density ceiling connects to the Greenwald-limit and radiative-boundary analysis [doi:10.5281/zenodo.22645947; greenwald-fraction-density-limit]; the ash-exhaust path is set by the stacked detachment portfolio [doi:10.5281/zenodo.22645742; divertor-portfolio] and the blanket/divertor thermal-hydraulics [doi:10.5281/zenodo.22645836; blanket-and-divertor-thermal-hydraulics]; the wall-chemistry choice that keeps bred tritium in the loop is the permeation-barrier-coating study [doi:10.5281/zenodo.22645870; tritium-permeation-barrier-coatings]. Downstream, the surplus tritium the breeder banks decays to the helium-3 that fuels the D–$^3$He burner, whose fuel-cycle closure is treated in the tritium-breeding ladder [doi:10.5281/zenodo.22645746; tritium-fuel-cycle-and-breeding-ladder] and the helium-3 supply analysis [doi:10.5281/zenodo.22645734; helium-3-fuel-cycle]; the fueling actuator itself is one controller in the breeder real-time control suite [doi:10.5281/zenodo.22645809; real-time-control-suite].

§ 8

# Limitations

The pellet-peaking benefit is quantified here as a scaling argument: equation (14) gives the fusion-rate gain for a given peaking factor $p$, and the NGS scaling of equation (16) estimates the penetration depth of a given pellet, but the step that closes the loop—converting a deposited profile into the achieved steady-state $p$ and the associated confinement time—requires a self-consistent core particle-transport calculation with the anomalous pinch [19] resolved on the negative-triangularity turbulence. BR-CX-09 flags exactly this as requiring a dedicated transport code [1], and the one-dimensional solver of §4 is built to consume the turbulent $D_s, v_s$ from that code once run. Until then, the peaking gain is an upper-bound scaling, not a predicted operating value; the source-to-exhaust budget of §2 and the exhaust and dilution relations of §3, which do not depend on the peaking closure, stand on the frozen anchors.

§ 9

# Conclusion

The Hyperion breeder's particle balance closes from source to exhaust at the frozen design point. The core burns D–T at $6.0 \times 10^{19}\,\mathrm{s}^{-1}$ and makes helium ash at $3.0 \times 10^{19}\,\mathrm{s}^{-1}$ with $99.99\%$ alpha confinement (table 1); the operating density is capped at $f_G \approx 0.36$ ( $\bar{n} = 4.8 \times 10^{20}\,\mathrm{m}^{-3}$) by the first-wall neutron budget rather than by the $f_G \approx 0.45$ gas limit (figure 2); pellet injection adds core peaking within that ceiling, worth $g(p) = p^2/(2p-1)$ in fusion rate—$\times 1.33$ at $p = 2$, $\times 1.80$ at $p = 3$ (figure 5)—at fixed wall load; and the divertor must exhaust helium at the production rate, holding the effective ash confinement time below $\tau^*_{\mathrm{He}} \lesssim 8.7\,s$ for a $5\%$ ash fraction (figure 3), a requirement looser than dedicated exhaust experiments have already met. A flowing-lithium plasma-facing surface keeps the bred tritium in the loop through the exhaust, and the fueling rate is coordinated with the operating-current window rather than run open-loop. Fueling method, density ceiling, and ash exhaust are one coupled system, governed by the single wall-load constraint that also governs the rest of the machine.

Acknowledgments tocsectionAcknowledgments Part of the Kronos Fusion Energy 2026 design series. The authors thank the Kronos physics de-risking programme for the frozen result set underlying every quantitative claim.

Reproducibility. The particle-balance rates are derived from the frozen anchor $P_{\mathrm{fus}} = 85.04\,MW$ through equations (1)–(2); the density-ceiling, alpha-confinement, ash and pellet quantities are frozen results (BR-CX-09, BR-L1-A14, BR-L2-A20, BR-L1-A6, KX-L1-A21, BR-SX-15, BR-SX-03) in the Kronos Physics De-Risking Register [1], doi:10.5281/zenodo.22133057. Every figure is regenerated byte-for-byte by the deposited script `make_fueling_ash_figs_2p45.py`. This paper is archived at its DOI doi:10.5281/zenodo.22645848; official version: https://www.kronosfusionenergy.com/publications/pellet-fueling-particle-balance-and-helium-ash-exhaust-.html and its official page is kronosfusionenergy.com/publications/pellet-fueling-particle-balance-and-helium-ash-exhaust.

Data availability tocsectionData availability The balance inputs and figure scripts are archived with the deposit at doi:10.5281/zenodo.22645848 and reference the Kronos 2026 series and its Physics De-Risking Register (doi:10.5281/zenodo.22133057). All quantitative values trace to the register by the serial identifiers cited inline. Any economic analysis is reported separately and is not part of the public deposit.

Competing interests tocsectionCompeting interests Provisional patent applications relating to aspects of this work have been filed.

tocsectionReferences

APPARATUS

# *Portfolio, People & Record*

*The intellectual-property estate, the people who built it, the limitations that gate it, and the sources it rests on.*

| 1 | 4 | 40 | 27 |
|---|---|---|---|
| GRANTED PATENT | 2026 PROVISIONALS | TEAM MEMBERS | 2022 PROVISIONALS |

INTELLECTUAL PROPERTY

# The patent portfolio

The estate spans a granted high-field magnet patent, pending utility and 2026 provisional filings that map to the two products, a digital-twin control provisional, a registered trademark application, and the original 2022 provisional family. Every patentable disclosure in the five-paper arXiv drop was protected **before** publication: the breeder and burner provisionals were filed 1–2 August, and a publication-gap omnibus filing the evening before the drop swept up the DEC, plasma-control, and REBCO-winding matter of the three otherwise-unprotected papers. Patent numbers and application serials are matters of public record; claim scope is summarised, not reproduced.

## GRANTED & PENDING UTILITY

| | | |
|---|---|---|
| US 12,009,112 | High-field tilted graded-REBCO magnet architecture (KRONO-002A) · *app. 17/878,550* | GRANTED |
| US 17/878,507 | Core device / method (KRONO-001A) · *utility* | PENDING |

## 2026 PROVISIONAL FILINGS — MAPPED TO THE PRODUCTS

| | | |
|---|---|---|
| 64/124,209 | Hyperion — spherical-tokamak tritium / helium-3 foundry · *breeder · filed Aug 2026* | FILED |
| 64/124,220 | Aegis / MetroVolt — synchrotron-cutoff, fuel-selection & plug-winding · *generator · filed Aug 2026* | FILED |
| 64/115,167 | KRONOS-CTRL digital-twin plant control · *provisional · filed Jul 2026* | FILED |
| 64/005,440 | Integrated spherical-tokamak fusion architecture · *early integrated-architecture filing · filed Mar 2026* | FILED |
| 64/105,530 | Negative-triangularity spherical-tokamak architecture · *foundational ST filing · filed Jul 2026* | FILED |
| 64/128,097 | Publication-gap omnibus — quasineutral two-species expander DEC · provenance-gated / latency-split plasma control · as-built high-field winding & conductor architecture · *filed 7 Aug 2026, the evening before the arXiv drop* | FILED |

## TRADEMARK & ORIGIN

| | | |
|---|---|---|
| FTK-98801894 | Kronos Fusion Energy — trademark application | FILED |
| KR-2022-* | Original provisional family (KR-2022-00001 … 00027) · *27 filings, 2022* | PRIORITY |

The narrow, defensible magnet novelty — the specific conductor and the digital-twin winding optimisation, not high-field REBCO as a category — is the commercial core that can earn ahead of any Q > 1 milestone, with markets in fusion magnet supply, MRI/NMR, accelerators, and proton therapy. The claim is scoped honestly: the high field is a *system field* result, not a stand-alone-coil record; the small-bore plug coil is structurally infeasible as a bare winding but resolved by a stress-managed structural shield (feasible-pending-FEA); and the winding-tape experiment returned a *null result*. The value is the method, not a field record.

THE TEAM

# Founding partners, board, advisors & auditors

Kronos is built by a bench of advanced-fuel-fusion, high-field-magnet, direct-conversion, and materials specialists, with a board and operations team drawn from defense, national laboratories, and industry. Dates are shown as ranges; where a tenure has ended or is term-ending, the range says so.

## FOUNDING PARTNERS — SCIENCE

**Dr. Gerald Kulcinski**
Co-Founder · Helium-3 & Advanced-Fuel Fusion
*UW–Madison · 2023–Present*

**Dr. Carl Weggel**
Chief Scientist / S.M.A.R.T. Design
*MIT Alcator Program · 2022–Present*

**Dr. Robert J. Weggel**
Magnetic Field Design
*MIT Magnet Lab · 2022–Present*

## BOARD

**Priyanca Ford**
Founder & CEO · Executive Board
*2022–Present*

**Bandel Carano**
Finance / Strategy
*Oak Investment Partners / Stanford · 2025–2026*

**Patrick Schweiger**
Fusion Device Engineering
*Oklo / CFS / TerraPower · 2025–Present*

## SCIENTIFIC ADVISORS

**Dr. Steven O. Dean**
Fusion Policy & History
*DOE / Fusion Power Associates · 2025–Present*

**Dr. Patrick H. Diamond**
Plasma Turbulence & Transport
*UC San Diego · 2025–Present*

**Dr. Jack J. Dongarra**
HPC & Numerical Algorithms
*Turing Award · 2025–Present*

**Dr. Nasr M. Ghoniem**
Chief Material Scientist
*UCLA · 2025–Present*

**Dr. Siegfried Glenzer**
Plasma Physics & Laser Fusion
*Stanford / SLAC · 2022–Present*

**Dr. David A. Hammer**
Pulsed-Power Fusion
*Cornell · 2025–Present*

**Dr. Donald A. Spong**
Plasma Theory & Confinement
*ORNL · 2025–Present*

**Dr. Curtis Smith**
Risk Assessment & Nuclear PRA
*MIT / Idaho National Lab · 2025–Present*

**RADM (Ret.) David Goggins**
Naval Engineering & Power-Plant Design
*U.S. Navy · 2023–2026*

**Dr. Konstantin Batygin**
Mathematician
*Caltech · 2022–2025*

**Dr. Ruben Fair**
Magnet Design / ITER Liaison
*PPPL / Jefferson Lab · 2022–2025*

**Dr. Paul S. Weiss**
Materials & Nanotechnology
*UCLA · 2022–2025*

## SCIENTIFIC AUDITORS

**Dr. Wilfred A. Cooper**
Plasma Equilibrium Theory
*EPFL / Swiss Plasma Center · 2025–Present*

**Dr. Ahmed Hassanein**
Plasma–Material Interactions
*Purdue / Argonne · 2025–Present*

**Dr. Patrick E. Hopkins**
Extreme Thermal Materials
*U. of Virginia · 2025–Present*

**Dr. Peter Hosemann**
Materials Joining & Structural Integrity
*UC Berkeley · 2025–Present*

**Dr. Travis W. Knight**
Advanced Nuclear Fuels & Systems
*U. of South Carolina · 2025–Present*

**Dr. Philippe Lebrun**
Cryogenics & Magnet Cooling
*CERN · 2025–Present*

**Dr. Nitendra Singh**
Nuclear Safety & Fuel Cycle
*ITER · 2025–Present*

**Dr. Guido Van Oost**
Magnetic Confinement & Fusion Systems
*Ghent University · 2025–Present*

**Dr. Gary S. Was**
Radiation Materials & Structural Integrity
*U. of Michigan · 2025–Present*

**Dr. Ray Sedwick**
Direct Energy Conversion
*U. of Maryland · 2025*

## OPERATIONS

**Michael Laughlin**
Chief Operating Officer
*2022–Present*

**Martin Owens**
Chief Strategy Officer
*LANL / GE Hitachi · 2022–Present*

**MG (Ret.) Paul Pardew**
Chief Contracting Officer
*Army Contracting Command · 2022–Present*

**David Beck**
Fusion Commercialization
*U.S. Space Force · 2024–Present*

**Sushma Bhatia**
Environmental & Legislative
*Google · 2022–Present*

**Michael De Frenza**
Technology Licensing
*2023–Present*

**MG (Ret.) Robin L. Fontes**
Cybersecurity & Defense
*Army Cyber Command · 2022–Present*

**Vijay Gehani**
Supply Chain & Components
*INOX India · 2024–Present*

**Jon Michel Greenwood**
IT & AI Infrastructure
*Live Nation · 2023–Present*

**Brian C. O'Neill**
National Security
*CIA / ODNI · 2022–Present*

**Gen. (Ret.) Gustave F. Perna**
DoD Liaison
*Operation Warp Speed · 2022–2023*

**Andrea Romero**
Marketing Lead
*2022–Present*

Legal counsel is retained; those roles are held on the internal roster and are not listed here.

SOURCES

# References


1 P I Ford, *Kronos Physics De-Risking Register*, Kronos Fusion Energy 2026 series. doi:10.5281/zenodo.22133057

2 J E Menard *et al*, Fusion nuclear science facilities and pilot plants based on the spherical tokamak, *Nucl. Fusion* **56** 106023 (2016). doi:10.1088/0029-5515/56/10/106023

3 B N Sorbom *et al*, ARC: a compact, high-field, fusion nuclear science facility and demonstration power plant with demountable magnets, *Fusion Eng. Des.* **100** 378 (2015). doi:10.1016/j.fusengdes.2015.07.008

4 A J Creely *et al*, Overview of the SPARC tokamak, *J. Plasma Phys.* **86** 865860502 (2020). doi:10.1017/S0022377820001257

5 M E Austin *et al*, Achievement of reactor-relevant performance in negative triangularity shape in the DIII-D tokamak, *Phys. Rev. Lett.* **122** 115001 (2019). doi:10.1103/PhysRevLett.122.115001

6 A Marinoni, O Sauter and S Coda, A brief history of negative triangularity tokamak plasmas, *Rev. Mod. Plasma Phys.* **5** 6 (2021). doi:10.1007/s41614-021-00054-0

7 M Greenwald, Density limits in toroidal plasmas, *Plasma Phys. Control. Fusion* **44** R27 (2002). doi:10.1088/0741-3335/44/8/201

8 H-S Bosch and G M Hale, Improved formulas for fusion cross-sections and thermal reactivities, *Nucl. Fusion* **32** 611 (1992). doi:10.1088/0029-5515/32/4/I07

9 P B Parks and R J Turnbull, Effect of transonic flow in the ablation cloud on the lifetime of a solid hydrogen pellet in a plasma, *Phys. Fluids* **21** 1735 (1978). doi:10.1063/1.862088

10 S L Milora, W A Houlberg, L L Lengyel and V Mertens, Pellet fuelling, *Nucl. Fusion* **35** 657 (1995). doi:10.1088/0029-5515/35/6/I04

11 B P\'egouri\'e, Review: pellet injection experiments and modelling, *Plasma Phys. Control. Fusion* **49** R87 (2007). doi:10.1088/0741-3335/49/8/R01

12 L R Baylor, T C Jernigan, S K Combs *et al*, Improved core fueling with high field side pellet injection in the DIII-D tokamak, *Phys. Plasmas* **7** 1878 (2000). doi:10.1063/1.874011

13 P T Lang *et al*, ELM pacing and high-density operation using pellet injection in the ASDEX Upgrade all-metal-wall tokamak, *Nucl. Fusion* **54** 083009 (2014). doi:10.1088/0029-5515/54/8/083009

14 D Reiter, G H Wolf and H Kever, Burn condition, helium particle confinement and exhaust efficiency, *Nucl. Fusion* **30** 2141 (1990). doi:10.1088/0029-5515/30/10/012

15 D Reiter *et al*, Helium removal from tokamaks, *Plasma Phys. Control. Fusion* **33** 1579 (1991). doi:10.1088/0741-3335/33/13/008

16 D L Hillis *et al*, Helium exhaust and transport studies with the ALT-II pump limiter in the TEXTOR tokamak, *Phys. Rev. Lett.* **65** 2382 (1990). doi:10.1103/PhysRevLett.65.2382

17 M R Wade, D L Hillis, J T Hogan *et al*, Helium exhaust studies in H-mode discharges in the DIII-D tokamak using an argon-frosted divertor cryopump, *Phys. Rev. Lett.* **74** 2702 (1995). doi:10.1103/PhysRevLett.74.2702

18 ITER Physics Basis Editors, Chapter 4: Power and particle control, *Nucl. Fusion* **39** 2391 (1999). doi:10.1088/0029-5515/39/12/304

19 C Angioni *et al*, Particle transport in tokamak plasmas, theory and experiment, *Plasma Phys. Control. Fusion* **51** 124017 (2009). doi:10.1088/0741-3335/51/12/124017

20 J Varje, K S\"arkim\"aki, J Kontula *et al*, High-performance orbit-following code ASCOT5 for Monte Carlo simulations in fusion plasmas, *Comput. Phys. Commun.* (2019), arXiv:1908.02482.

21 S Wiesen *et al*, The new SOLPS-ITER code package, *J. Nucl. Mater.* **463** 480 (2015). doi:10.1016/j.jnucmat.2014.10.012

22 D Reiter, M Baelmans and P B\"orner, The EIRENE and B2-EIRENE codes, *Fusion Sci. Technol.* **47** 172 (2005). doi:10.13182/FST47-172

23 P K Romano *et al*, OpenMC: a state-of-the-art Monte Carlo code for research and development, *Ann. Nucl. Energy* **82** 90 (2015). doi:10.1016/j.anucene.2014.07.048

24 J Candy, E A Belli and R V Bravenec, A high-accuracy Eulerian gyrokinetic solver for collisional plasmas, *J. Comput. Phys.* **324** 73 (2016). doi:10.1016/j.jcp.2016.07.039

25 K L van de Plassche, J Citrin, C Bourdelle *et al*, Fast modeling of turbulent transport in fusion plasmas using neural networks, *Phys. Plasmas* **27** 022310 (2020). doi:10.1063/1.5134126

26 F Felici *et al*, Real-time physics-model-based simulation of the current density profile in tokamak plasmas, *Nucl. Fusion* **51** 083052 (2011). doi:10.1088/0029-5515/51/8/083052

27 L L Lao, H St John, R D Stambaugh, A G Kellman and W Pfeiffer, Reconstruction of current profile parameters and plasma shapes in tokamaks, *Nucl. Fusion* **25** 1611 (1985). doi:10.1088/0029-5515/25/11/007

28 J Degrave *et al*, Magnetic control of tokamak plasmas through deep reinforcement learning, *Nature* **602** 414 (2022). doi:10.1038/s41586-021-04301-9

COLOPHON

# How this document was made

*The Kronos Fleet — Combined Editorial, 2026* is set in **Fraunces** (display), **Gelasio** (text), and **IBM Plex Mono** (data & equations), carried forward from the Kronos editorial design system.

The figures are rendered at 300 dpi from the deposited generator scripts; the document is composed as a single self-contained file with embedded fonts and imagery, paginated to US Letter, and rendered to PDF through a headless Chromium engine in matched light and dark editions.

Every headline quantity carries an evidence class; withdrawn and restated values are marked as such. Nothing herein is frozen beyond the founder-approved Tier-A set.

Explore it live — turn the interactive 3-D model, run the deposited solvers in the physics validator, and watch the companion film series.

LEGAL NOTICE

# Notice, status, and distribution

**Conceptual design & simulation study.** This document reports a conceptual design and simulation study. It is not a construction commitment, a safety-analysis report, a regulatory filing, or an offer of securities. Forward-looking statements — schedules, costs, market sizes, and performance — are estimates subject to the limitations set out in the Simulations part and may change.

**Numbers and their classes.** Quantities are reported with evidence classes and case labels; modelled, assumed, and requirement-class values are identified as such and are not to be quoted without their labels.

**Public edition.** This edition carries the physics and design only; all financial, funding, and defense-commercial content has been removed for public distribution. The scientific text corresponds to the arXiv and journal submissions.

THE 2026 KRONOS SERIES

# One programme, many papers

This editorial is one paper in the Kronos 2026 series — a real fusion company's complete, reproducible physics record for a spherical-tokamak breeder and its low-neutron D–$^3$He tandem-mirror burners. Every headline number is a frozen anchor in the Physics De-Risking Register.

Explore the whole programme: the De-Risking Register, the interactive 3-D model, and the physics validator.

KRONOS FUSION ENERGY

# *Pellet Fueling, Particle Balance, and Helium-Ash Exhaust for Sustained Burn in a Compact Spherical-Tokamak Breeder*

A real fusion company building real machines. Explore the science, live.

Zenodo · doi:10.5281/zenodo.22645848

Read on kronosfusionenergy.com

The Physics De-Risking Register